Original article

Macromolecules: Synthesis, antimicrobial, POM analysis and computational approaches of some glucoside derivatives bearing acyl moieties

Mohammad R. Kayes [a], Supriyo Saha [b], Mohammed M. Alanazi [c,*], Yasuhiro Ozeki [d], Dilipkumar Pal [e], Taibi B. Hadda [f], Abdelkhaleq Legssyer [f], Sarkar M.A. Kawsar [a,*]

[a] Laboratory of Carbohydrate and Nucleoside Chemistry, Department of Chemistry, Faculty of Science, University of Chittagong, Chittagong 4331, Bangladesh
[b] Uttaranchal Institute of Pharmaceutical Sciences, Uttaranchal University, Dehradun, Uttarakhand 248007, India
[c] Department of Pharmaceutical Chemistry, College of Pharmacy, King Saud University, P.O. Box 2457, Riyadh 11451, Saudi Arabia
[d] School of Sciences, Yokohama City University, 22-2, Seto, Kanazawa-Ku, Yokohama 236-0027, Japan
[e] Department of Pharmaceutical Sciences, Guru Ghasidas Vishwavidyalaya (A Central University), C.G., 495009 Bilaspur, India
[f] BBEH and LACE Laboratories of Applied Chemistry & Environment, Faculty of Sciences, Mohammed Premier University, MB 524, 60000 Oujda, Morocco

ARTICLE INFO

ABSTRACT

Macromolecules i.e., carbohydrate derivatives are crucial to biochemical and medical research. Herein, we designed and synthesized eight methyl α-D-glucopyranoside (MGP) derivatives (2–8) in good yields following the regioselective direct acylation method. The structural configurations of the synthesized MGP derivatives were analyzed and verified using multiple physicochemical and spectroscopic techniques. Antimicrobial experiments revealed that almost all derivatives demonstrated noticeable antifungal and antibacterial efficacy. The synthesized derivatives showed minimum inhibitory concentration (MIC) values ranging from 0.75 µg/mL to 1.50 µg/mL and minimum bactericidal concentrations (MBCs) ranging from 8.00 µg/mL to 16.00 µg/mL. Compound 6 inhibited Ehrlich ascites carcinoma (EAC) cell proliferation by 10.36% with an IC50 of 2602.23 µg/mL in the MTT colorimetric assay. The obtained results were further rationalized by docking analysis of the synthesized derivatives against 4URO and 4XE3 receptors to explore the binding affinities and nonbonding interactions of MGP derivatives with target proteins. Compound 6 demonstrated the potential to bind with the target with the highest binding energy. In a stimulating environment, a molecular dynamics study showed that MGP derivatives have a stable conformation and binding pattern. The MGP derivatives were examined using POM (Petra/Osiris/Molinspiration) bioinformatics, and as a result, these derivatives showed good toxicity, bioavailability, and pharmacokinetics. Various antifungal/antiviral pharmacophore ($O^{\delta-}$, $O'^{\delta-}$) sites were identified by using POM investigations, and compound 6 was further tested against other pathogenic fungi and viruses, such as Micron and Delta mutants of SARS-CoV-2.

1. Introduction

Carbohydrates are known to form glycoproteins when combined with proteins and glycolipids when combined with lipids (Bertozzi and Kiessling, 2001). Carbohydrates are found in DNA (deoxyribonucleic acid) and RNA (ribonucleic acid), which are fundamental polymers of D-ribose-phosphate and 2-deoxy-D-ribose phosphate to which purine and pyrimidine bases are linked at the C-1 position. Carbohydrates are globally accepted as several groups of compounds that are omnipresent in nature. Approximately 75% of the dry weight of the plant is technically a carbohydrate; it consists of mainly cellulose, hemicellulose and lignin (Chen and Fukuda, 2006). The significance of carbohydrates (aside from the direct benefits) is that they offer an additional benefit; carbohydrate breakdown through various foods leads to the consumption of other needed nutrients. Thus, it is advisable to seek out unique sources of carbohydrates in the diet. Additionally, carbohydrates are regarded as a source of biofuel that powers essen-

* Corresponding authors.
  E-mail addresses: mmalanazi@ksu.edu.sa (M.M. Alanazi), akawsarabe@yahoo.com (S.M.A. Kawsar).
Peer review under responsibility of King Saud University.

tial biochemical activities such as metabolism (Varki, 1993; Seeberger and Werz, 2007). Carbohydrate molecule investigations have offered surprising results in the fields of medicinal chemistry, and their derivatives have been found to have good antibacterial, antifungal, antiprotozoal, antitumor, anti-inflammatory, antidiabetic and antineoplastic activities against human and plant pathogenic microorganisms (Joshi et al., 2023; Kabir et al., 2004, 2009; Saha et al., 2021). Since ancient times, scientists have become interested in carbohydrates because of their broad relevance in the biomedical sector with regard to bacterial, viral, and fungal infections as well as cell proliferation (Berredjem et al., 2020; Jordheim et al., 2012; Judge et al., 2013).

According to a reliable literature review, a variety of biologically active compounds contain substituents such as aromatic rings (halobenzoyl, nitrobenzoyl, alkylbenzoyl, and acybenzoyl), heteroaromatic rings, and aliphatic chains (Bulbul et al., 2021; Kawsar et al., 2011; Misbah et al., 2020; Shagir et al., 2016). It was shown that the biochemical and biological activity of compounds based on carbohydrates can be greatly increased by benzene rings, substituted benzene rings, —NO2, S, and X-based groups, among other things. (Hosen et al., 2022; Konze et al., 2019; Kuzmanic and Zagrovic, 2010). It was also found that the biological potential of a molecule can be enhanced by connecting the active moiety with an aromatic and heterocyclic part. This connection is considered a crucial factor in the process (Hasan et al., 2022; Kawsar et al., 2011; Mahmud et al., 2021a, 2021b; Maowa et al., 2021a, 2021b). According to a study on the regioselective acylation of carbohydrate derivatives and their antimicrobial activities (Farhana et al., 2021a, 2021b), attaching two or more highly electron-rich heteroaromatic nuclei and aliphatic chains significantly improves the derivatives' antimicrobial activity compared to the parent nucleus (Banerjee et al., 2018; Bechlem et al., 2010; Daina et al., 2017; Mahmud et al., 2021a, 2021b; Kawsar and Kumer 2021).

Inspired by the abovementioned, a series of MGP derivatives were synthesized with different acylating agents inserted at positions 6, 2, 3 and 4 in methyl α-D-glucopyranoside structures to synthesize novel MGP derivatives. The *in vitro* antimicrobial evaluation of several MGP-based derivatives **2–8** with different aliphatic and aromatic chains against seven pathogens, molecular docking analyses against the 4URO and 4XE3 receptors along with ADMET (absorption, distribution, metabolism, excretion, and toxicity), antiproliferative effects and cytotoxicity are reported herein. To confirm the stability of the docked complexes, molecular dynamics was performed for 100 ns. Furthermore, we analyzed the POM studies of MGP derivatives **2–8** to identify their pharmacophore sites for the first time.

2. Materials and methods

2.1. Materials and chemical reagents

Unless otherwise stated, all reagents were used precisely as received and were commercially available (Aldrich). ^{1}H NMR spectra (400 MHz) and ^{13}C NMR spectra (100 MHz) were recorded for solutions in deuteriochloroform (CDCl$_3$) unless specified, (internal Me$_4$Si) with a Bruker spectrospin spectrometer at BCSIR Laboratories, Dhaka.

2.2. Synthesis of glucoside derivatives

2.2.1. Methyl 6-O-(triphenylmethyl)-α-D-glucopyranoside (2)

A solution of methyl α-D-glucopyranoside (**1**) (100 mg, 0.515 mmoL) in dry (CH$_3$)$_2$NC(O)H (DMF: dimethylformamide) (4 mL) was cooled to 0 °C and treated with 1.1 M equivalents of triphenyl-

methyl chloride (0.162 g) with continuous stirring while maintaining the °C temperature for six hours [4-dimethylaminopyridine (DMAP)/tryethylamine (TEA)]. Stirring continued at ambient temperature overnight. The contents of the flask were extracted three times with ten milliliters of CHCl3 after a few pieces of ice were placed in the flask to remove the surplus reagent. The obtained thick liquid was separated by silica gel column chromatography with CH$_3$OH-CHCl$_3$ (1:24) to yield title compound **2** as a needle.

Yield (109 mg, 79.12%), white solid, m.p. 122–125 °C. FTIR ν_{max} (KBr): 1689 (—CO), 3405–3501 (br, —OH) cm^{-1}; ^{1}H NMR (400 MHz, CDCl$_3$) δ_H ppm H 7.70 (6H, m, Ar—H), 7.32 (9H, m, Ar—H), 4.91 (1H, d, *J* = 3.4 Hz, H-1), 4.76 (1H, dd, J = 5.2 and 12.2 Hz, H-6a), 4.55 (1H, dd, J = 2.1 and 12.1 Hz, H-6b), 3.94 (1H, t, *J* = 9.2 Hz, H-3), 3.90 (1H, t, *J* = 9.5 Hz, H-4), 3.76 (1H, dd, J = 3.3 and 10.0 Hz, H-2), 3.62 (1H, ddd, J = 2.8, 9.6 and 12.8 Hz, H-5), 3.21 (3H, s, 1-OCH$_3$); ^{13}C NMR (100 MHz, CDCl$_3$) δ_C ppm 137.09 (×3), 133.05, 129.69, 129.26 (×2), 129.18 (×3), 126.11 (×3), [(C$_6$H$_5$)$_3$C—], 101.83 [(C$_6$H$_5$)$_3$C—], 99.56 (C-1), 77.34 (C-2), 77.02 (C-4), 76.70 (C-3), 76.48 (C-5), 70.03 (C-6), 68.81 (1-OCH$_3$); LC-MS [M + 1]$^+$: 437.4801; Anal. Calcd for C$_{26}$H$_{28}$O$_6$: C, 71.50; H, 6.40. Found: C, 71.52; H, 6.41%.

2.3. General procedure for the synthesis of methyl 6-O-(triphenylmethyl)-α-D-Glucopyranoside derivatives (3–6)

Ttriphenylmethyl derivative (**2**) (80 mg, 0.15 mmoL) in DMF was cooled to 0 °C, and lauryl chloride (0.07 mL) was added in the presence of TEA. Lauryl derivative **3** was obtained as a crystalline solid after enduring purification by chromatography with CH$_3$OH-CHCl$_3$ (1:24) as the eluent. Compounds **4–6** were synthesized and obtained as needles using similar reaction and purification techniques.

2.3.1. Methyl 2,3,4-tri-O-lauryl-6-O-(triphenylmethyl)-α-D-glucopyranoside (3)

Yield (91.23 mg, 96.17%), white solid, m.p. 127–128 °C. FTIR ν_{max} (KBr): 1701 (C=O) cm^{-1}; ^{1}H NMR (400 MHz, CDCl$_3$) δ_H ppm 7.74 (6H, m, Ar—H), 7.38 (9H, m, Ar—H), 5.01 (1H, d, *J* = 3.3 Hz, H-1), 4.97 (1H, dd, J = 3.4 and 10.0 Hz, H-2), 4.90 (1H, t, *J* = 9.4 Hz, H-3), 4.51 (1H, t, *J* = 9.5 Hz, H-4), 4.37 (1H, dd, J = 2.1 and 12.1 Hz, H-6b), 3.61 (1H, dd, J = 4.6 and 10.2 Hz, H-6a), 3.58 (1H, m, H-5), 3.38 (3H, s, 1-OCH$_3$), 2.36 {6H, m, 3 × CH$_3$(CH$_2$)$_9$CH$_2$-CO—}, 1.65 {6H, m, 3 × CH$_3$(CH$_2$)$_8$CH$_2$CH$_2$CO—}, 1.28 {48H, m, 3 × CH$_3$(CH$_2$)$_8$CH$_2$CH$_2$CO—}, 0.90 {9H, m, 3 × CH$_3$(CH$_2$)$_{10}$CO—}; ^{13}C NMR (100 MHz, CDCl$_3$) δ_C ppm 172.50, 172.48, 172.46 {3 × CH$_3$(CH$_2$)$_{10}$CO—}, 145.44, 145.21(×2), 129.04(×6), 127.86 (×3), 126.77(×6) [(C$_6$H$_5$)$_3$C—], 81.35 [(C$_6$H$_5$)$_3$C—], 97.11 (C-1), 72.90 (C-2), 71.34 (C-4), 71.04 (C-3), 69.11 (C-5), 63.12 (C-6), 55.11 (1-OCH$_3$), 34.38, 34.12 (×2), 31.90 (×3), 29.59 (×3), 29.45, 29.32 (×2), 29.24 (×3), 29.15, 25.01 (×2), 24.96, 22.67(×3), 22.65, 22.62 (×3), 21.72, 21.69, 20.09 (×2) {3 × CH$_3$(CH$_2$)$_{10}$CO—}, 13.51, 13.50, 13.48 {3 × CH$_3$(CH$_2$)$_{10}$CO—}; LC-MS [M + 1]$^+$: 984.4204; Anal. Calcd for C$_{62}$H$_{94}$O$_9$: C, 75.65; H, 9.56. Found: C, 75.64; H, 9.57%.

2.3.2. Methyl 2,3,4-tri-O-myristoyl-6-O-(triphenylmethyl)-α-D-glucopyranoside (4)

Yield (95 mg, 96.43%), white solid, m.p. 118–120 °C. FTIR ν_{max} (KBr): 1707 (C=O) cm^{-1}; ^{1}H NMR (400 MHz, CDCl$_3$) δ_H ppm 7.68 (6H, m, Ar—H), 7.31 (9H, m, Ar—H), 5.07 (1H, d, *J* = 3.4 Hz, H-1), 4.99 (1H, dd, J = 3.2 and 10.1 Hz, H-2), 4.93 (1H, t, *J* = 9.3 Hz, H-3), 4.57 (1H, t, *J* = 9.5 Hz, H-4), 4.41 (1H, dd, J = 2.2 and 12.1 Hz, H-6b), 3.74 (1H, dd, J = 4.5 and 10.2 Hz, H-6a), 3.68 (1H, m, H-5), 3.39 (3H, s, 1-OCH$_3$), 2.39 {6H, m, 3 × CH$_3$(CH$_2$)$_{11}$CH$_2$CO—}, 1.66 {6H, m, 3 × CH$_3$(CH$_2$)$_{10}$CH$_2$CH$_2$CO—}, 1.27 {48H, m, 3 × CH$_3$(CH$_2$)$_{10}$-CH$_2$CH$_2$CO—}, 0.88 {9H, m, 3 × CH$_3$(CH$_2$)$_{12}$CO—}; ^{13}C NMR (100 MHz, CDCl$_3$) δ_C ppm 172.54, 172.48, 172.40 {3 × CH$_3$(CH$_2$)$_{12}$-

CO—}, 145.22 (×2), 145.18, 129.55, 129.52 (×5), 127.23 (×3), 127.04 (×6) [(C₆H₅)₃C—], 81.13 [(C₆H₅)₃C—], 97.02 (C-1), 72.91 (C-2), 71.34 (C-4), 70.66 (C-3), 69.41 (C-5), 63.11 (C-6), 55.12 (1-OCH₃), 34.38, 34.36, 34.12 (×2), 31.92, 31.90 (×2), 29.59 (×2), 29.45, 29.37, 29.32 (×2), 29.24 (×3), 29.15, 25.01 (×2), 24.96, 24.92, 22.67(×3), 22.65, 22.64(×3), 22.62 (×3), 21.72, 21.69, 20.09 (×2), 20.07 {3 × CH₃(CH₂)₁₂CO—}, 14.08, 14.05, 14.01 {3 × CH₃(CH₂)₁₂CO—}; LC-MS [M + 1]⁺: 1062.5311; Anal. Calcd for C₆₈H₁₀₀O₉: C, 76.87; H, 9.42. Found: C, 76.89; H, 9.41%.

2.3.3. Methyl 2,3,4-tri-O-(4-t-butylbenzoyl)-6-O-(triphenylmethyl)-α-D-glucopyranoside (5)

Yield (129 mg, 76.07%), white solid, m.p. 101–102 °C. FTIR ν_max (KBr): 1711 (C=O) cm⁻¹; ¹H NMR (400 MHz, CDCl₃) δ_H ppm 8.07 (6H, m, Ar—H), 7.70 (6H, m, Ar—H), 7.55 (6H, m, Ar—H), 7.32 (9H, m, Ar—H), 5.43 (1H, d, J = 3.6 Hz, H-1), 5.01 (1H, dd, J = 3.5 and 10.6 Hz, H-2), 4.89 (1H, t, J = 9.1 Hz, H-3), 4.71 (1H, t, J = 9.5 Hz, H-4), 4.62 (1H, m, H-6a), 4.51 (1H, m, H-6b), 3.98 (1H, m, H-5), 3.36 (3H, s, 1-OCH₃), 1.32 {27H, s, 3×(CH₃)₃C—}; ¹³C NMR (100 MHz, CDCl₃) δ_C ppm 174.40, 174.23, 174.11 {3×(CH₃)₃CC₆H₄-CO—}, 146.0 (×3), 130.01 (×6), 127.11 (×3), 127.02 (×6) [(C₆H₅)₃C—], 81.30 [(C₆H₅)₃C—], 132.44 (×3), 132.40 (×2), 132.40, 130.94 (×3), 129.91 (×3), 126.52 (×3), 125.50 (×3) {3×(CH₃)₃CC₆-

H₄CO—}, 97.01 (C-1), 72.93 (C-2), 71.35 (C-4), 70.61 (C-3), 69.33 (C-5), 63.01 (C-6), 55.12 (1-OCH₃); 35.60, 35.57, 35.41 {(×3)(CH₃)₃-CC₆H₄CO—}, 13.67 (×3), 13.65 (×3), 13.42 (×3) {(×3)(CH₃)₃CC₆H₄-CO—}; LC-MS [M + 1]⁺: 918.1002; Anal. Calcd for C₅₉H₆₄O₉: C, 77.29; H, 6.90%. Found: C, 77.28; H, 6.91%.

2.3.4. Methyl 2,3,4-tri-O-(bezenesulphonyl)-6-O-(triphenylmethyl)-α-D-glucopyranoside (6)

Yield (155 mg, 74.15%), white solid, m.p. 111–112 °C. FTIR ν_max (KBr): 1713 (C=O), 1368 (-SO₂) cm⁻¹; ¹H NMR (400 MHz, CDCl₃) δ_H ppm 7.75 (6H, m, Ar—H), 7.71 (6H, m, Ar—H), 7.66 (3H, m, Ar—H), 7.53 (6H, m, Ar—H), 7.36 (9H, m, Ar—H), 5.18 (1H, d, J = 3.6 Hz, H-1), 5.18 (1H, dd, J = 3.7 and 10.1 Hz, H-2), 5.0 (1H, t, J = 9.5 Hz, H-3), 4.81 (1H, m, H-4), 4.22 (1H, m, H-6a), 4.09 (1H, dd, J = 2.1 and 12.1 Hz, H-6b), 3.91 (1H, m, H-5), 3.38 (3H, s, 1-OCH₃); ¹³C NMR (100 MHz, CDCl₃) δ_C ppm 145.55 (×3), 129.76 (×6), 127.65 (×3), 127.51 (×6) [(C₆H₅)₃C—], 81.27 [(C₆H₅)₃C—], 144.35, 144.28, 144.07, 135.40, 135.17, 135.02, 129.79 (×3), 129.11 (×3),126.90 (×3), 126.45 (×3) (×3C₆H₅SO₂−); 97.21 (C-1), 72.55 (C-2), 71.23 (C-4), 70.59 (C-3), 69.29 (C-5), 63.13 (C-6), 55.44 (1-OCH₃); LC-MS [M + 1]⁺: 857.9608; Anal. Calcd for C₄₄H₄₀S₃O₁₂: C, 61.61; H, 4.67. Found: C, 61.60; H, 4.66%.

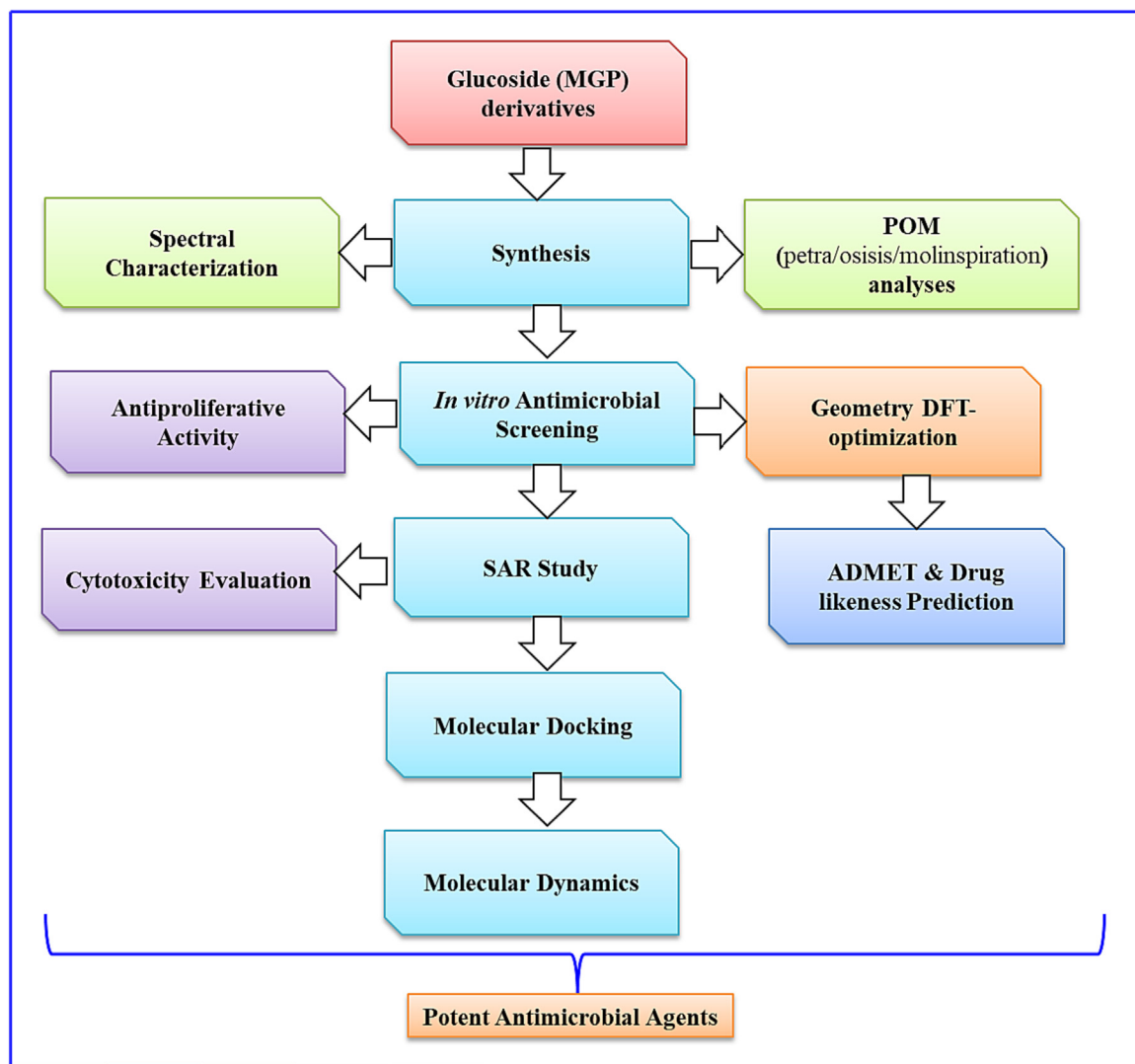**Fig. 1.** Flow diagram of the whole study.

2.3.5. Methyl 6-O-(4-methoxybenzoyl)-α-D-glucopyranoside (7)

Methyl α-D-glucopyranoside (**1**) (100 mg, 0.515 mmol) was dissolved in anhydrous DMF (3 mL) and cooled to 0 °C before adding 4-methoxybenzoyl chloride (0.12 mL, 1.1 M eq.) with DMAP. The samples were stirred at 0 °C for four hours and at room temperature overnight. A conventional work-up procedure followed by chromatographic purification with CH_3OH-$CHCl_3$ (1:12) as the eluent afforded the 4-methoxybenzoyl derivative (**7**). A similar experimental and work-up procedure was applied to prepare compound **8**.

Yield (127 mg, 76.90%), white solid, m.p. 108–109 °C. FTIR ν_{max} (KBr): 1700 (—CO), 3402–3497 (br —OH) cm^{-1}; ^{1}H NMR (400 MHz, CDCl$_3$) δ_H ppm 8.05 (H, d, J = 8.4 Hz, Ar—H), 7.42 (H, d, J = 8.1 Hz, Ar—H), 7.28 (H, d, J = 8.4 Hz, Ar—H), 6.93 (H, d, J = 7.5 Hz, Ar—H), 5.52 (1H, d, J = 3.7 Hz, H-1), 5.35 (1H, dd, J = 5.1 and 12.1 Hz, H-6a), 4.71 (1H, dd, J = 2.1 and 12.2 Hz, H-6b), 4.38 (1H, t, J = 9.1 Hz, H-3), 4.24 (1H, t, J = 9.5 Hz, H-4), 4.22 (1H, dd, J = 3.7 and 10.0 Hz, H-2), 4.20 (1H, ddd, J = 2.8, 9.8 and 12.7 Hz, H-5), 3.88 (3H, s, Ar-OCH$_3$), 3.38 (3H, s, 1-OCH$_3$); ^{13}C NMR (100 MHz, CDCl$_3$) δ_C ppm 166.98 (CH$_3$OC$_6$H$_4$CO—), 165.50, 133.98 (×2), 125.31, 114.31 (×2) (CH$_3$OC$_6$H$_4$CO-), 55.77 (CH$_3$OC$_6$H$_4$CO—), 97.17 (C-1), 72.90 (C-2), 71.18 (C-4), 70.43 (C-3), 69.71 (C-5), 63.19 (C-6), 55.22 (1-OCH$_3$); LC-MS [M + 1]$^{+}$: 329.2913; Anal. Calcd for C$_{15}$H$_{20}$O$_8$: C, 54.82; H, 5.50. Found: C, 54.80; H, 5.51%.

2.3.6. Methyl 2,3,4-tri-O-lauroyl-6-O-(4-methoxybenzoyl)-α-D-glucopyranoside (8)

Yield (103 mg, 94.96%), white solid, m.p. 110–112 °C. FTIR ν_{max} (KBr): 1713 (C=O) cm^{-1}; ^{1}H NMR (400 MHz, CDCl$_3$ δ_H ppm 8.04 (H, d, J = 8.5 Hz, Ar—H), 7.71 (H, d, J = 8.1 Hz, Ar—H), 7.54 (H, d, J = 8.4 Hz, Ar—H), 6.93 (H, d, J = 7.5 Hz, Ar—H), 5.21 (1H, d, J = 3.3 Hz, H-1), 4.96 (1H, dd, J = 3.4 and 10.0 Hz, H-2), 4.91 (1H, t, J = 9.4 Hz, H-3), 4.90 (1H, t, J = 9.5 Hz, H-4), 4.58 (1H, dd, J = 2.1 and 12.1 Hz, H-6b), 4.55 (1H, dd, J = 4.6 and 10.2 Hz, H-6a), 3.88 (3H, s, Ar-OCH$_3$), 3.51 (1H, m, H-5), 3.21 (3H, s, 1-OCH$_3$), 2.35 (6H, m, 3 × CH$_3$(CH$_2$)$_9$CH$_2$CO-), 1.66 (6H, m, 3 × CH$_3$(-CH$_2$)$_8$CH$_2$CH$_2$CO-), 1.31 (48H, m, 3 × CH$_3$(CH$_2$)$_8$CH$_2$CH$_2$CO-), 0.91 (9H, m, 3 × CH$_3$(CH$_2$)$_{10}$CO-); ^{13}C NMR (100 MHz, CDCl$_3$) δ_C ppm 172.50, 172.48, 172.46 {3 × CH$_3$(CH$_2$)$_{10}$CO—},166.66 (CH$_3$OC$_6$H$_4$-CO—), 165.52, 133.75(×2), 125.30, 114.22(×2) (CH$_3$OC$_6$H$_4$CO-), 55.62 (CH$_3$OC$_6$H$_4$CO—); 97.17 (C-1), 72.88 (C-2), 71.12 (C-4), 70.55 (C-3), 69.41 (C-5), 63.22 (C-6), 55.11 (1-OCH$_3$), 34.38, 34.12 (×2), 31.90 (×3), 29.59 (×3), 29.45, 29.32 (×2), 29.24 (×3), 29.15, 25.01 (×2), 24.96, 22.67(×3), 22.65, 22.62 (×3), 21.72,
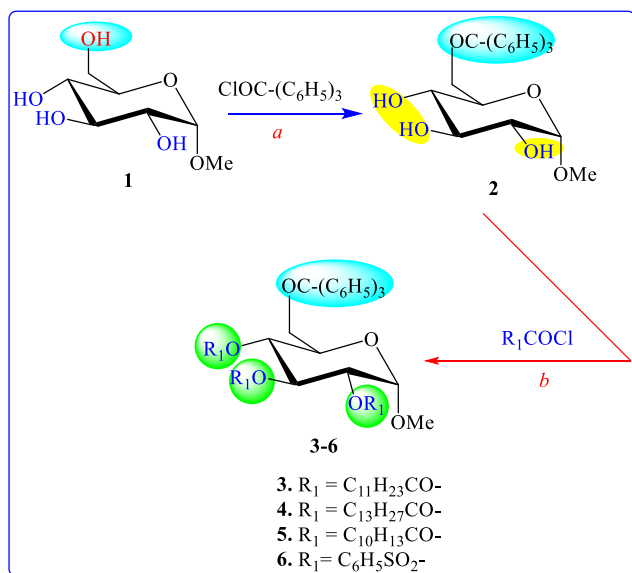
Scheme 1A. General procedure for synthesizing derivatives **2–6** (MGP, **1**); (*a*) dry DMF, 0 °C, 6 h; DMAP, R$_1$ = triphenylmethyl chloride; (*b*) R$_1$ = different acyl halides under the same conditions (**3–6**).
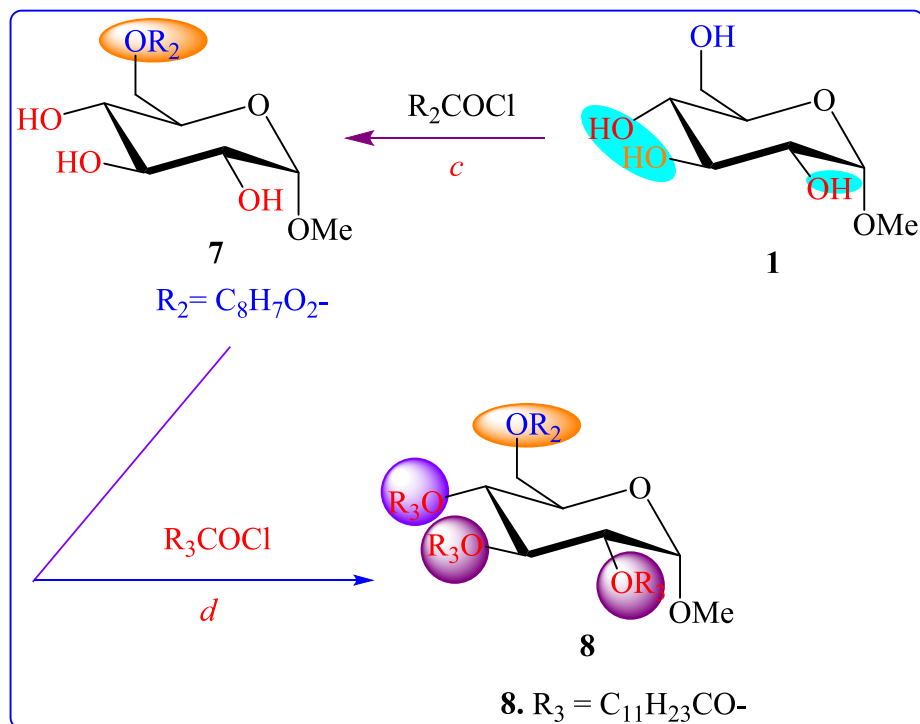
Scheme 1B. General procedure for synthesizing derivatives **7–8** (MGP, **1**); (*c*) dry DMF, 0 °C, 6 h, R$_2$ = 4-methoxybenzoyl chloride; (*d*) R$_3$ = lauroyl halide.

21.69, 20.09 (×2) {3 × $CH_3(CH_2)_{10}CO—$}, 13.51, 13.50, 13.48 {3 × $CH_3(CH_2)_{10}CO—$}; LC-MS $[M + 1]^+$: 876.2206; Anal. Calcd for $C_{51}H_{86}O_{11}$: C, 69.92; H, 9.83. Found: C, 69.93; H, 9.82%.

2.4. Antimicrobial screening

Test chemicals comprising partially protected derivatives of MGP (**2**–**8**) were utilized. A total of five human pathogenic bacteria and two plant pathogenic fungi were utilized for antimicrobial screening, as illustrated in Table S1.

2.4.1. Antibacterial activity

The *in vitro* antibacterial activities of the synthesized MGP derivatives (**2**–**8**) were determined by the disc diffusion method (Bauer et al., 1966). Standard nutrient agar (NA) was used as the basal medium for antibacterial tests throughout the study.

2.4.2. Microbroth dilution method for MIC and MBC

The minimum inhibitory concentration (MIC) and the minimum bactericidal concentration (MBC) of two test compounds (**5** and **6**) against the tested microorganisms were investigated by the Clinical and Laboratory Standards Institute (CLSI) method (CLSI, 2012).

2.4.3. Screening of mycelial growth

MGP derivatives (2–8) were tested for *in vitro* antifungal activity against two plant pathogenic fungi. The investigation was based on the poisoned food technique (Grover and Moore, 1962).

2.5. Antiproliferative activity

The MTT colorimetric assay (Islam et al., 2022) was used to determine the *in vitro* antiproliferative activity of compounds **1**–**8** against Ehrlich ascites carcinoma (EAC) cells. The cells (5×10^5) were seeded in 200 μL RPMI-1640 medium in 96-well plates with different concentrations of compound **6** and incubated for 24 h at 37 °C, 5% CO_2 and 100% relative humidity.

2.6. Structure–activity relationship (SAR)

Structure–activity relationship (SAR) analysis was performed to identify the active component of the synthesized molecule. According to the membrane permeation concept of (Ingólfsson and Andersen, 2011), this well-known technique is frequently employed in the drug design process.

Table 1
Antibacterial screening for gram-positive and gram-negative bacteria.

| Entry | Diameter of Inhibition Zones (in mm) | | | | |
	B. subtilis (G + ve)	*S. aureus* (G + ve)	*E. coli* (G–ve)	*S. typhi* (G–ve)	*P. aeruginosa* (G–ve)
1	NI	NI	NI	NI	NI
2	8 ± 0.5	NI	9 ± 0.2	NI	9 ± 0.1
3	NI	NI	NI	10 ± 0.1	*12 ± 0.3
4	10 ± 0.3	NI	NI	9 ± 0.5	8 ± 0.2
5	*13 ± 0.4	*17 ± 0.1	*15 ± 0.2	10 ± 0.4	NI
6	*14 ± 0.5	*15 ± 0.3	*12 ± 0.3	*14 ± 0.5	*17 ± 0.5
7	*12 ± 0.2	10 ± 0.1	9 ± 0.4	NI ± 0.1	NI
8	9 ± 0.3	11 ± 0.2	10 ± 0.1	NI ± 0.3	NI
Azithromycin	**19 ± 0.6	**18 ± 0.5	**17 ± 0.4	**19 ± 0.5	**17 ± 0.5

All experimental triplicate values are shown. Asterisks (*) and double asterisks (**) indicate significant inhibition ($p < 0.05$). NI = No inhibition.
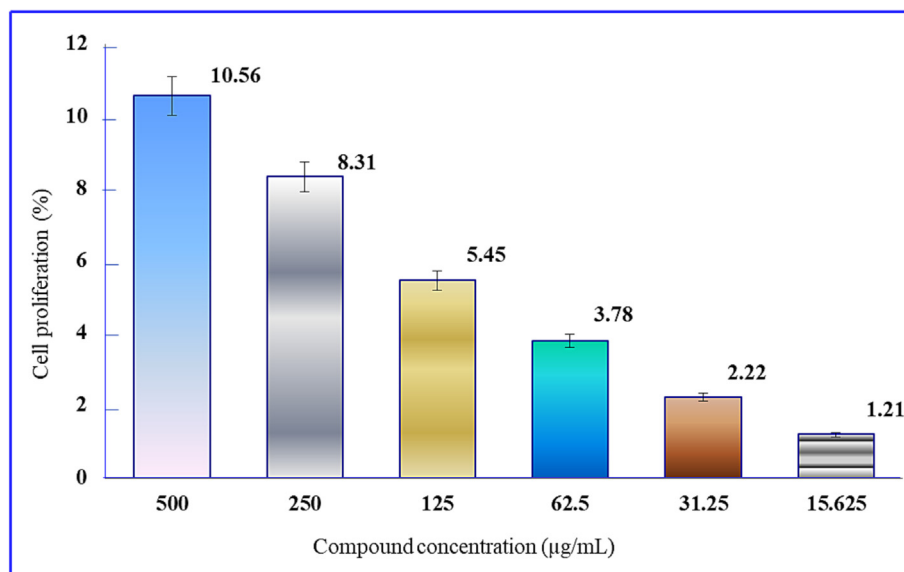

Fig. 2. Inhibition of EAC cell growth after treatment with MGP derivative **6**.

2.7. Cytotoxic activity evaluation

The toxicity of glucopyranoside (MGP) derivatives was evaluated using the brine shrimp lethality assay (BSLA) technique as outlined by McLaughlin (1991). The evaluated MGP derivatives were dissolved in DMSO and prepared at four different concentrations: 20, 40, 80, and 160 μL. This was achieved by adding 5 mL of NaCl solution to each vial. The vials labeled A, B, C, and D contained sample concentrations of 4, 8, 16, and 32 μL, respectively. The experiment was conducted in triplicate for every concentration, and each vial was inoculated with 10 brine shrimp nauplii. The mortality rate of nauplii was determined for each concentration, and the average percentage was calculated. No fatalities were observed within the control group.

2.8. Molecular docking, protein selection and visualization

In a molecular docking study, ligands and proteins interact with each other to produce a best-fitted interactive pose (Opoku et al., 2019; Saha et al., 2010). In this study, synthesized molecules were docked against 4URO and 4XE3 receptors to evaluate their antibacterial and antifungal activities, respectively. The 4URO receptor is the crystal structure of staph gyrase-B, belonging to the *Staphylococcus aureus* organism, and *Escherichia coli* BL21 (DE3) as an expression system. The receptor is composed of four chains with 231 amino acids on each chain. In 4URO, novobiocin is present

within the receptor as a cocrystallized ligand. The 4XE3 receptor is the crystal structure of the cytochrome P450 epoxidase receptor obtained from *Streptomyces antibioticus* and *Escherichia coli* BL21 (DE3) as an expression system. In 4XE3, clotrimazole is present in the receptor as a complex ligand molecule (Ahmad et al., 2020; Raies and Bajic, 2016). Swiss PDB viewer software was used for energy minimization of the proteins. The H++ server was then used to preserve the ionization state of the receptor's existing amino acids after receptors had been verified for missing residues using PyMol software. After that, Drug Discovery Studio was used to assess the cocrystallized ligands' surrounding residues. The MGL software package's AutodockVina and AutoDock Tools (ADT) were used for docking analysis and converting pdb format into Pdbqt format in both proteins and ligands.

2.9. Molecular dynamic simulations

The thermodynamic properties of the ligand-receptor complex were studied using GROMACS 20.1 on LINUX UBUNTU. Two independent procedures were taken to process the energy minimized utilizing the steepest descent technique with a 100 ns MD (molecular dynamics) simulation run. The initial phase kept the pressure, temperature, and particle parameters constant while keeping the number of particles, volume, and temperature (nvt) constant. A total of 100,000 energy-saving steps were carried out in this study. The GROMACS software suite was used to examine the MD simu-
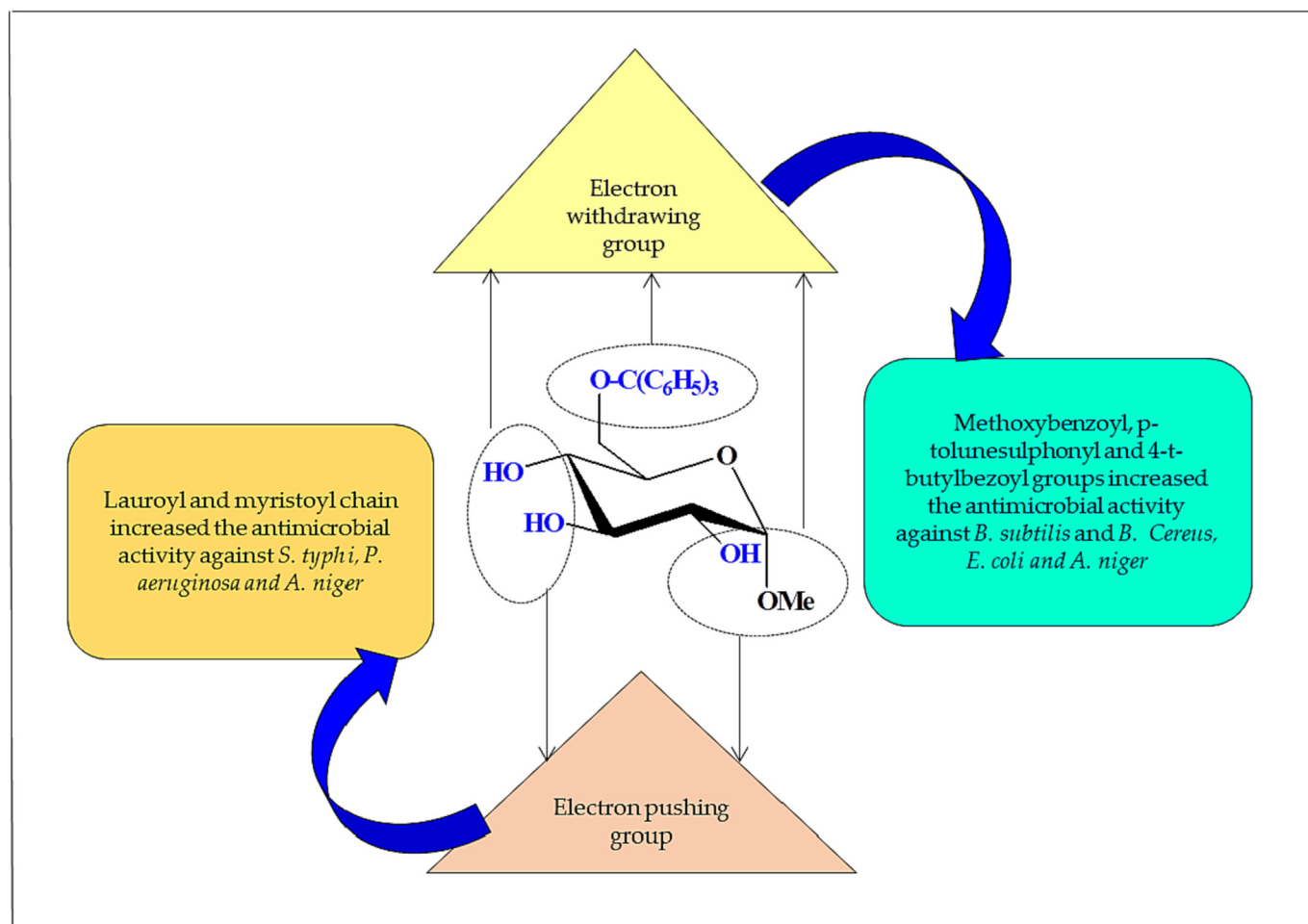

Fig. 3. SAR studies of MGP derivatives **2** against bacterial pathogens.

lation trajectory. Using the gmx rms and gmx rmsf software, the RMSD (root mean square standard deviation) and RMSF (root mean square fluctuation) of the protein–ligand complexes were calculated. Using the gmx sasa and gmx gyrate tools, the solvent accessible surface area (SASA) and radius of gyration (Rg) were calculated. The gmx h-bond tool was used to examine hydrogen bond formation. The graphical representation of the trajectories was plotted using the Qtgrace program (Rana et al., 2021).

2.10. ADMET profile

Drug-likeness probability, Log S, Log D, Log P, Log Papp (Caco-2 cell permeability), Pgp inhibitor, Pgp substrate, human intestine absorption, plasma protein binding, blood–brain barrier penetration, distribution volume, CYP450 1A2, 3A4, 2C9, 2C19, and 2D6 inhibitors, half-life T1/2, clearance, hERG blocker, human hepatotoxicity, AMES mutagenicity, skin sensitivity, LD50, drug-induced liver injury, maximum recommended daily dose, molecular

weight, hydrogen bond acceptor, donor, topological polar surface area, Chem AGG aggregator, and false positive probability data of all synthesized molecules were established employing ADMETlab (Singh and Siddiqi, 2017).

2.11. POM (petra/Osiris/molinspiration) study

The POM (Petra/Osiris/Molinspiration) theory emerged with the aim of identifying and optimizing pharmacophore sites for antibacterial (Hadda et al., 2013a, 2013b), antifungal (Mabkhot et al., 2014), antiviral (Rachedi et al., 2019), antiparasitic (Bhat et al., 2021), and antitumor (Bechlem et al., 2010) agents. POM theory, originally developed for a specific biotarget, has been expanded to encompass a range of diverse biotargets (Hadda et al., 2020). We are conducting an analysis on compounds 1–8 to determine the appropriate pharmacophore sites.
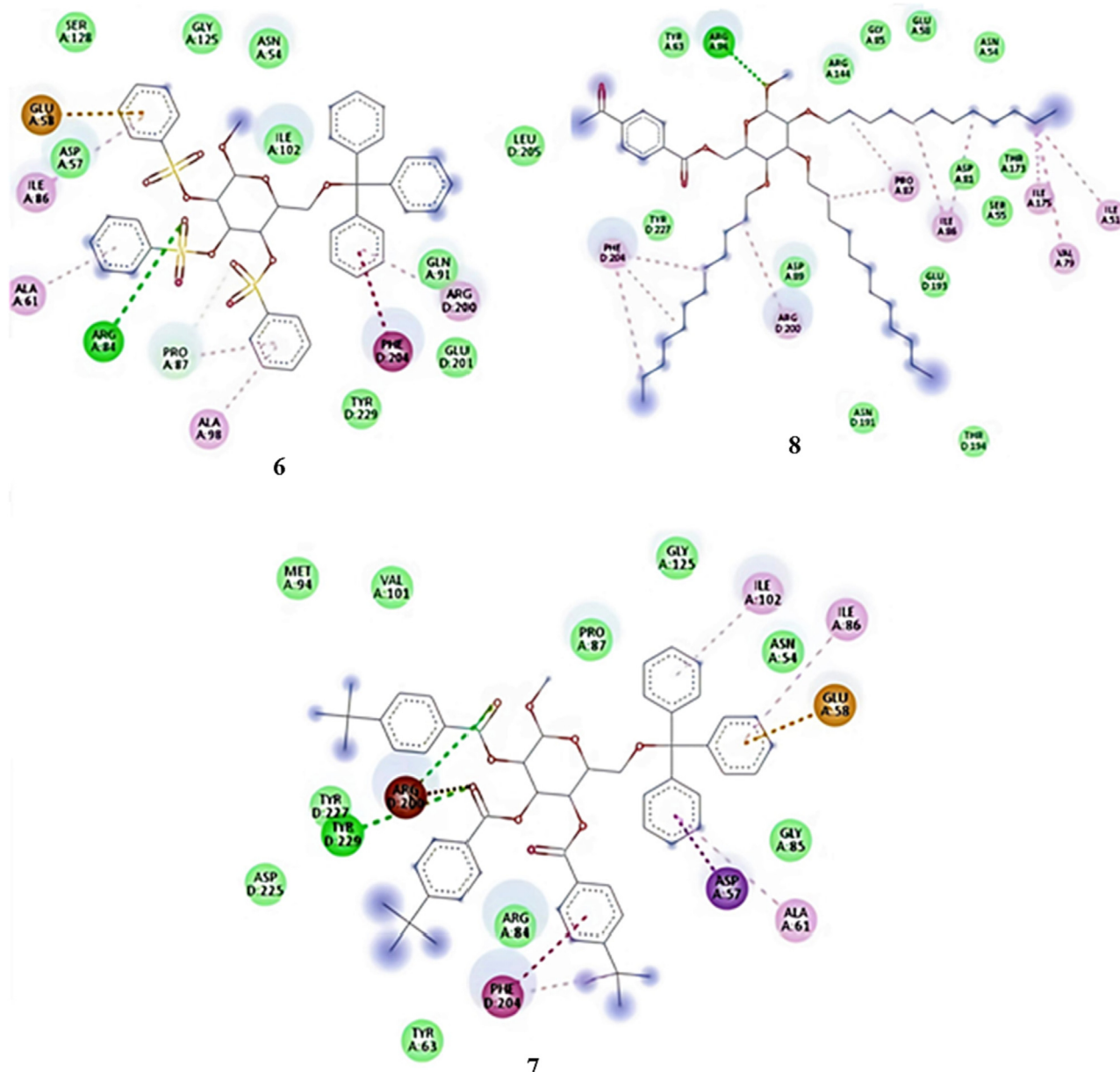
Fig. 4. Nonbonding interactions of compounds **6**, **8** and **7** with 4URO.

3. Results

3.1. Chemistry

Following the schematic flow in Fig. 1, derivatives 2–8 were successfully synthesized by selective tritylation (Scheme 1A) and 4-methoxybenzoylation (Scheme 1B) using a direct acylation method [50]. The identity of the chemical structures was confirmed by multiple spectroscopic methods (Table S1 and Figs. S1–S3).

3.2. Antibacterial screening

The results of the antibacterial tests for derivatives **1**–**8** against seven pathogens are displayed in Tables 1, S2 and Figs. S4 and S5.

3.3. Antifungal susceptibility

All derivatives were tested for their antifungal activity against *Aspergillus niger* and *Aspergillus flavus,* and the results are shown in Table 1.

3.4. MTT assay for anticancer activity

The antiproliferative activity of compounds **1**–**8** was investigated by MTT assay against EAC cells, and the results are depicted in Fig. 2.

3.5. Structure–activity relationship

The structure–activity relationship (SAR) was studied to explain MGP derivative antibacterial processes (Fig. 3).

3.6. Cytotoxic activity against saline shrimp

The cytotoxic effects of the synthesized MGP derivatives (**2**–**8**) in the saline shrimp lethality bioassay are depicted in Fig. S8.

3.7. Molecular docking

Molecular docking results against 4URO for the synthesized compounds **1**–**8** are shown in Table 3. Types of interactions for compounds **6**, **7** and 8 with URO are demonstrated in Fig. 4 and

Fig. 5. Nonbonding interactions of compounds **6** with 4XE3.

Fig. 6. MD simulation results of all the molecular complexes with 4URO.

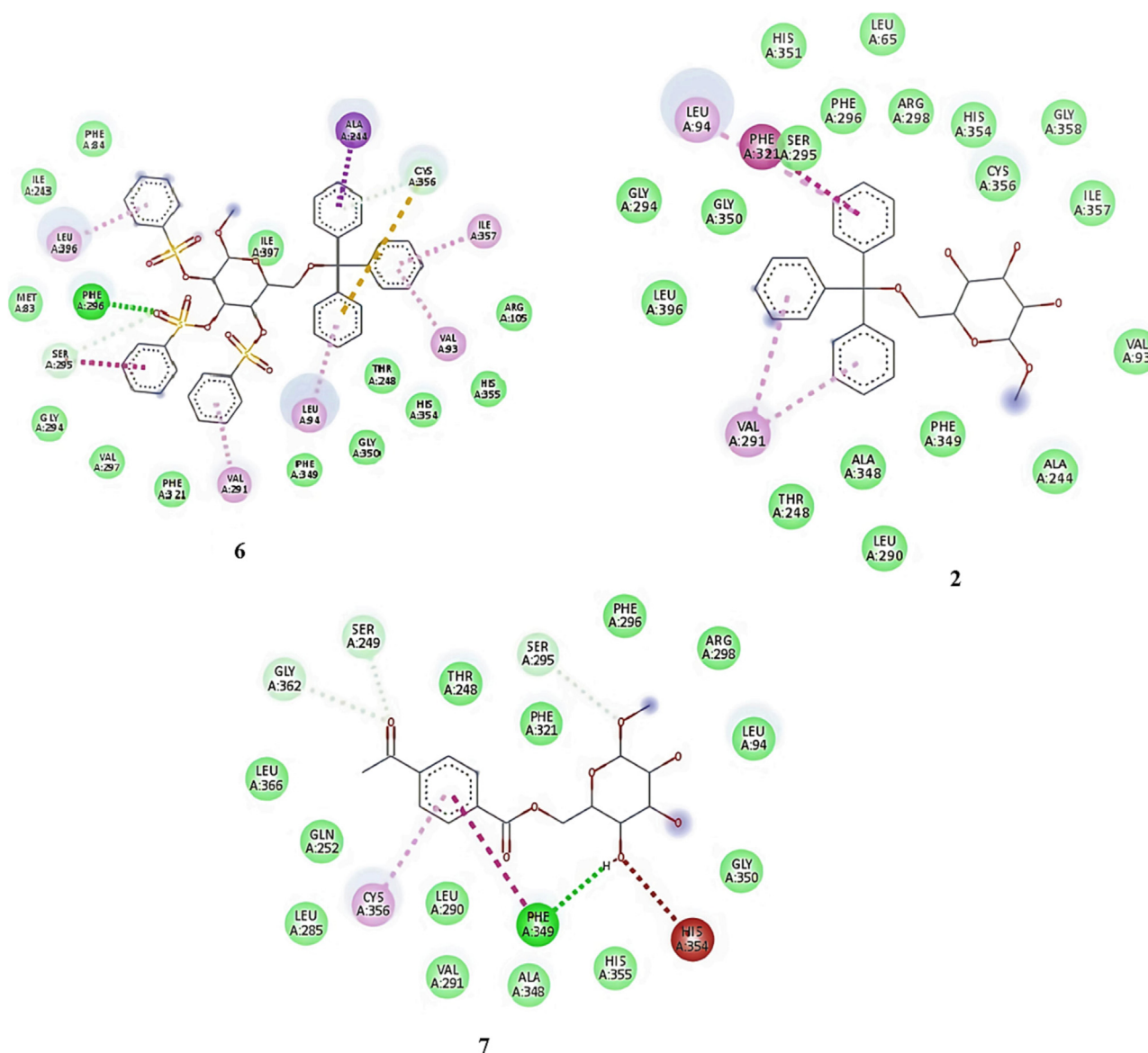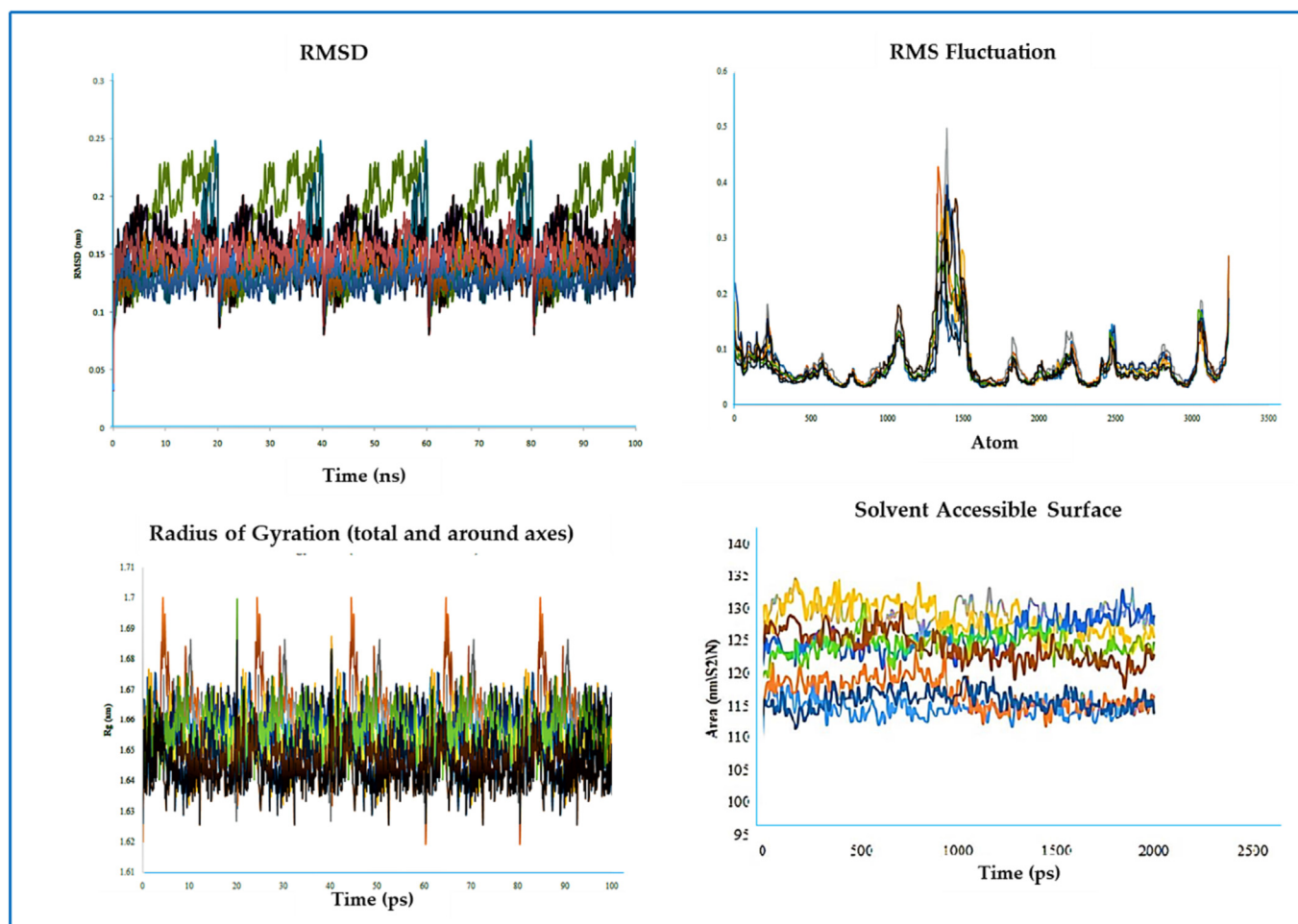for compound **6** with 4XE3 in Fig. 5 and Table S4. All the binding energies of the synthesized molecules docked with 4URO and 4XE3 have been inserted in Fig. S10. The validation of the receptor proteins was also assessed using the Lig-plot and Ramachandran plot through the PDBsum online server (Fig. S9).

3.8. Molecular dynamics (MD) simulation performance

The RMSD values of the 4URO and 4XE3-ligand complexes were found to be within 0.11–0.23 nm and 0.144–0.159 nm, respectively (Figs. 6 and 7).

3.9. ADMET exploration

In silico ADMET profiling of compounds **1–8** was investigated and is displayed in Table S5.

3.10. POM (petra/osiris/molinspiration)

The identification of the pharmacophore sites of the MGP derivatives was determined based on their physical and chemical properties using the Petra, Osiris, and Molinspiration (POM) interface (Fig. 8, Tables 4 and S6) (Grib et al., 2020).

3.11. Identification of combined antibacterial/antifungal/antiviral pharmacophore sites

The comparison between the pharmacophore of dithymoquinone, a promising anti-COVID-19 agent (Hadda et al., 2013a, 2013b, 2019), and the pharmacophore site of compound **6**, which exhibits antibacterial, antifungal, and antiviral properties, has been studied and is demonstrated in Figs. 9 and S11.

4. Discussion

The main goal of this research was to enact a selective tritylation (Scheme 1A) and 4-methoxybenzoylation (Scheme 1B) of methyl α-D-glucopyranoside (**1**) using a direct acylation method (Shagir et al., 2016). The initial step was to prepare the only intermediate in this research, namely, methyl 6-O-triphenylmethyl-α-D-glucopyranoside (**2**). For this purpose, the main attention was to carry out selective acylation of methyl α-D-glucopyranoside (**1**) with triphenylmethyl chloride in dry DMF at −5 °C. The work-up procedure was achieved by filtration and purification by column chromatography, and as a result, triphenylmethyl derivative (**2**) in 69.0% yield and a melting point of 122–125 °C was obtained and used for the next step. The FTIR spectrum showed characteristic peaks at 1689 (—CO) and 3405–3501 cm^{-1} (br, —OH stretching). The ^{1}H NMR spectrum showed two characteristic six-proton multiplets at δ 7.70 (Ar—H) and nine-proton multiplets at δ 7.32 (Ar—H) due to the three phenyl protons of the trityl group. The
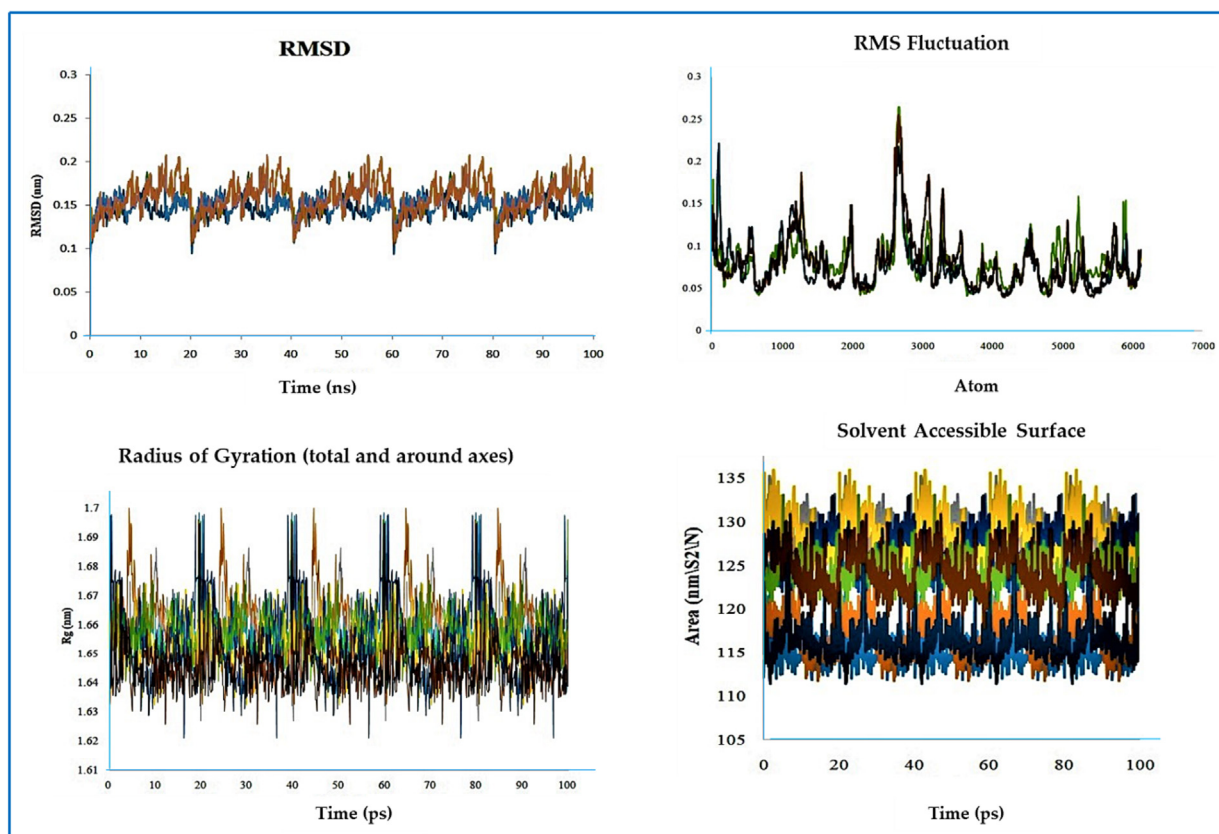
Fig. 7. MD simulation results of all the molecular complexes with 4XE3.

downfield shift of the C-6 protons to 4.76 (as dd, J = 5.2 and 12.2 Hz, H-6a) and 4.55 (as dd, J = 2.1 and 12.1 Hz, H-6b) from their precursor (**1**) values and the resonances of other protons in their predicted positions demonstrated attachment of the triphenylmethyl group at position 6. The ^{13}C NMR spectrum also supported the presence of one triphenylmethyl group by demonstrating all the characteristic peaks. The rest of the FTIR, ^{1}H NMR and other spectra were completely in compliance with the structure according to the trityl derivative as methyl 6-*O*-triphenylmethyl-α-D-glu copyranoside (**2**) (Fig. S1). The sterically less hindered primary hydroxyl group (Islam et al., 2022) of the ring may be more reactive, resulting in the synthesis of the 5-*O*-triphenylmethyl derivative (**2**) (Scheme 1A).

In addition, the structure was confirmed as methyl 6-*O*-(triphenyl methyl)-α-D-glucopyranoside by examining its COSY (correlation spectroscopy), HSQC (heteronuclear single quantum coherence), and HMBC (heteronuclear multiple bond correlation) spectral data as well as the ^{13}C NMR spectrum (**2**) (Table S1 and Fig. S2).

The structure of the triphenylmethyl derivative (**2**) was also determined by its transformation to and consolidation of its lauroyl derivative (**3**). Its ^{1}H NMR spectrum exhibited two six-proton multiplets at 2.36 {3 × CH$_3$(CH$_2$)$_9$C*H$_2$*CO─}, δ 1.65 {3 × CH$_3$(-CH$_2$)$_8$C*H$_2$*CH$_2$CO─}, a forty-eight-proton multiplet at δ 1.25 {3 × CH$_3$(C*H$_2$*)$_8$CH$_2$CH$_2$CO─} and a nine-proton multiplet at δ 0.90 {3 × C*H$_3$*(CH$_2$)$_{10}$CO─}, thereby suggesting the presence of three lauroyl groups. Further support for the structure of compound (**2**) was achieved by synthesizing its myristoyl (**4**), 4-*t*-butylbenzoate (**5**) and benzenesulfonyl (**6**) derivatives by the usual procedure with good yields (Scheme 1B).

4-Methoxybenzoate with methyl α-D-glucopyranoside **1** was obtained using 4-methoxybenzoyl chloride by applying direct acylation methods. The corresponding 4-methoxybenzoyl derivative

(**7**) was isolated in good yield. In its ^{1}H NMR spectrum, four characteristic doublets at δ 8.05, 7.42, 7.28, and 6.93 and a three-proton singlet at δ 3.88 indicated the presence of the 4-methoxybenzoyl group in compound **1**. The FTIR, ^{1}H- and ^{13}C NMR spectra of lauroate **8** admittedly displayed the formation of the 2,3,4-tri-*O*-lauroyl-product (**8**) (Fig. S3).

The antimicrobial results of compounds **1**–**8** revealed that compound **5** demonstrated the highest zone of inhibition against *B. cereus* (17 ± 0.1 mm) and *B. subtilis* (13 ± 0.4 mm), while compound **6** exhibited a considerable zone of inhibition against both *B. subtilis* (14 ± 0.5 mm) and *B. cereus* (15 ± 0.3 mm). Remarkably, compounds **7** and **8** exhibited a fluctuating zone of inhibition against both gram-positive pathogens. On the other hand, compound **3** did not show any inhibitory activity against the tested gram-positive bacteria. Furthermore, based on the data presented, derivative **6** revealed a zone of inhibition against all three gram-negative bacteria: *E. coli, S. typhi* and *P. aeruginosa*. Compounds **3** and **4** inhibited two bacteria: *P. aeruginosa* and *S. typhi*. In addition, during the assessment of antibacterial properties against pathogenic bacteria, the minimal inhibitory concentration (MIC) and minimal bactericidal concentration (MBC) values of the most potent derivatives (MGP, **1**) were determined (Table S3, Figs. S6 and S7) (Bulbul et al., 2021; Misbah et al., 2020). In fact, compounds **5** and **6** exhibited the most effective antibacterial properties against the tested strains, with minimum inhibitory concentration (MIC) values ranging from 0.25 to 2.0 μg/mL. Both compounds exhibited inhibitory activity against all tested bacteria. Compound **6** demonstrated the highest level of inhibitory activity against *P. aeruginosa*, with a recorded value of 0.25 μg/mL. For all derivatives, the lowest MBC value of 8.00 μg/mL was against *B. cereus*, while the highest MBC value of 16.00 μg/mL was observed for these compounds against *B. subtilis* and *E. coli*. The minimum bac-
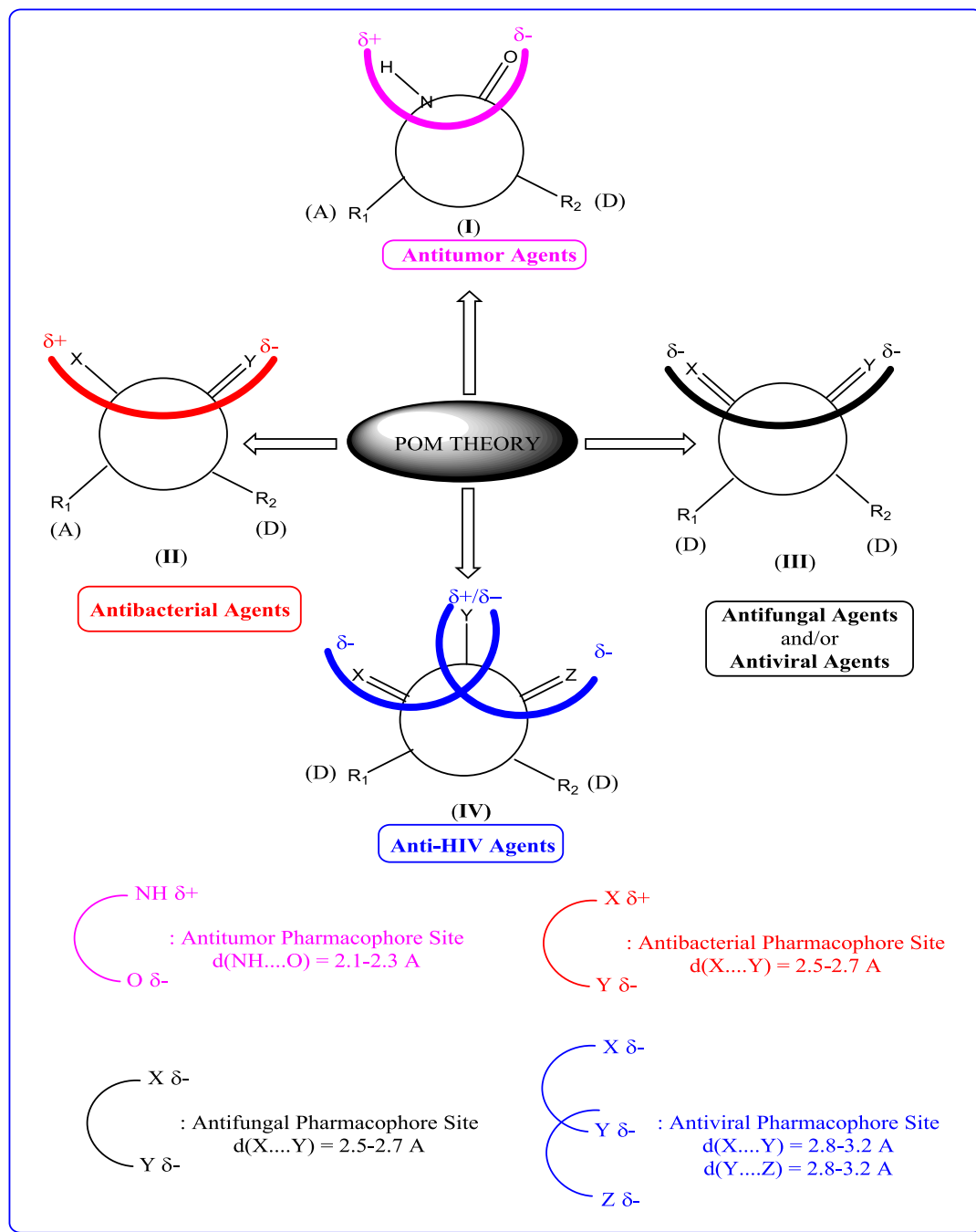
Fig. 8. Utilizing POM theory, the pharmacophore sites of different drug categories are determined and optimized.

tericidal concentration (MBC) values for these compounds, with respect to the other tested organisms, fall within the range of 8.0 0–16.00 µg/mL (Kabir et al., 2004, 2008; Sheikh and Hadda, 2013).

In addition, all derivatives constructed, including MGP **1**, exhibited significant inhibition of mycelial growth in both *A. niger* and *A. flavus*, as shown in Table 2. Among the tested derivatives, compound **6** inhibited 67.92% of *A. niger* and 66.46% of *A. flavus* in their potential antifungal assessment. Robust mycelial growth prevention was also observed for compounds **5** and **8** against *A. niger* (58.41% and 66.41% and 59.54% and 63.31%, respectively). Moreover, promising mycelial growth prevention was observed for compound **5** against *A. niger* (48.40%) in the mycelial growth test. Most of the compounds, excluding **4**, showed activity against both fungi. The zone of inhibition for compound **6** was higher than that of the

reference standard antifungal drug (nystatin) (Farhana et al., 2021b; Waring et al., 2002).

Moreover, the MTT assay was employed to examine the impact of *in vitro* anticancer activity on EAC cells following the screening of compounds **1**–**8**. The study revealed that EAC cell death occurred in a dose-dependent manner, as illustrated in Fig. 2. Compound **6** exhibited inhibitory effects of 10.36%, 8.31%, 5.45%, 3.78%, 2.22% and 1.21% at concentrations of 500, 250, 125, 62.5, 31.25 and 15.625 µg/mL, respectively. As the concentration gradually decreased, the corresponding inhibitory effect also decreased. The IC_{50} of compound **6** was determined to be 2602.23 g/mL.

On the other hand, structure–activity relationship (SAR) analysis explained MGP derivative antibacterial processes (Fig. 3). MGP (**1**) did not show any antibacterial activity. In general, compounds
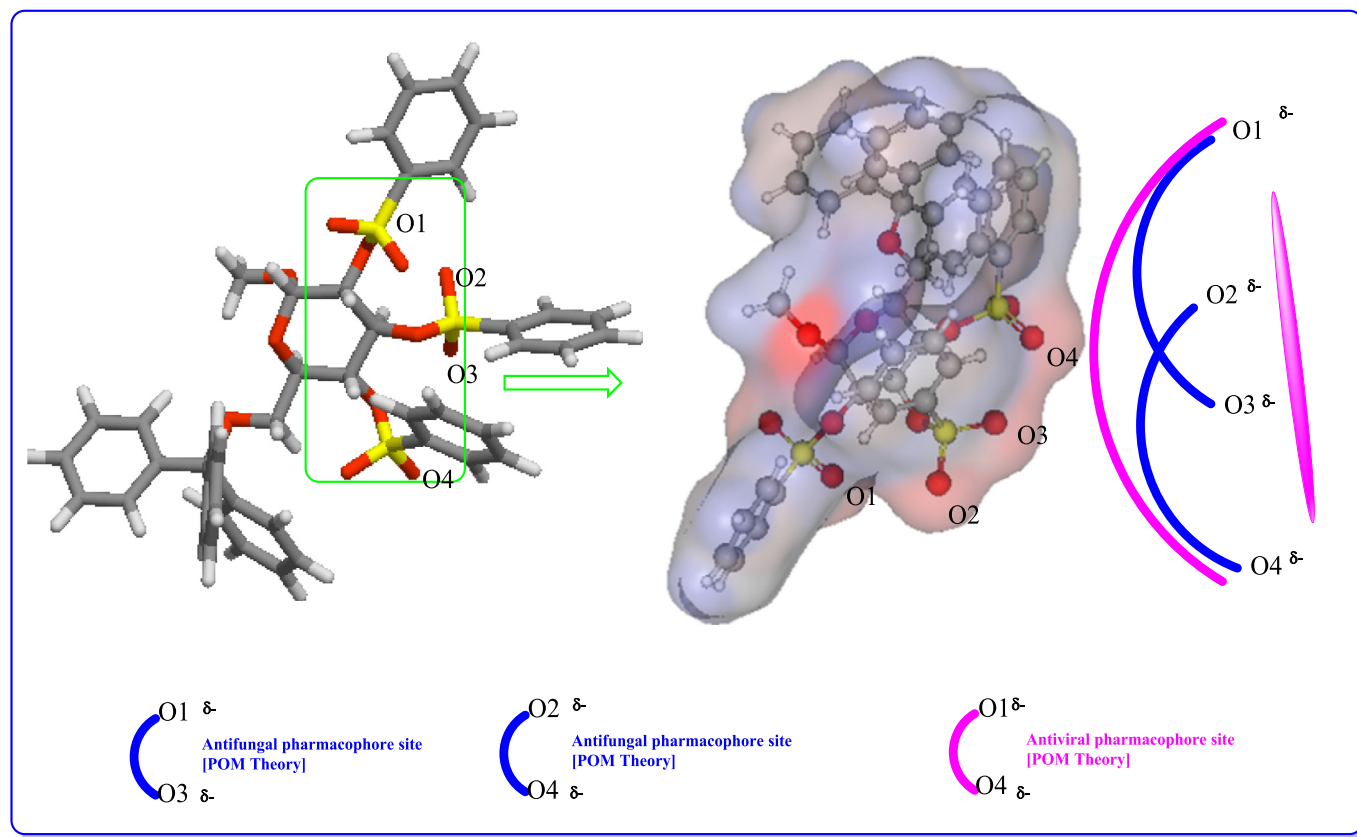
Fig. 9. Identification of potential antifungal/antiviral (O, O′) pharmacophore sites.

Table 2
Percent inhibition of fungal mycelial growth.

Entry	Millimeters of Fungal Mycelial Growth Inhibition in DMSO (20 µg/µL).	
	Aspergillus niger	*Aspergillus flavus*
1	NI	NI
2	36.43	33.33
3	46.62	41.30
4	31.92	NI
5	*58.41 ± 0.12	*59.54 ± 0.14
6	*67.92 ± 0.46	*66.46 ± 0.30
7	48.40 ± 0.22	35.38 ± 0.32
8	*66.41 ± 0.37	*63.31 ± 0.51
Nystatin	**66.40 ± 0.05	**63.10 ± 0.09

An asterisk * for test compounds: double asterisk ** for the reference antibiotic, * for the significant value, NI = No inhibition.

comprising a fused myristoyl moiety were more active than those comprising a ribose moiety for most tested bacteria. In contrast, the lauroyl-containing analog (**3**) was weaker than the myristoyl derivative (**4**). On the other hand, aromatic derivatives (**5**, **6** and **7**) were more active against all bacteria than aliphatic derivatives. The MIC values for the produced compounds in this investigation ranged from 0.25 to 2.0 mg/L, suggesting that gram-negative bacteria were more resistant to the compounds. Gram-positive and gram-negative bacteria likely behave differently, as they have distinct cell wall compositions. One possible reason for this is that the outer membrane surrounding the peptidoglycan of gram-negative bacteria prevents diffusion through the lipopolysaccharide (LPS) coating. As a highly effective barrier against the quick penetration of different chemicals, the LPS layer is crucial in enabling selective permeability. Hydrophobic interactions cause bacteria to lose

membrane permeability, which ultimately results in cell death (Ingólfsson and Andersen, 2011; Zhou and Wang, 2020; Li et al., 2010).

Furthermore, the cytotoxic effect of synthesized MGP derivatives (**2–8**) in the saline shrimp lethality bioassay method (Kawsar et al., 2008) is depicted in Fig. S8, which illustrates the percentage of dead shrimp after 24 and 48 h. Long alkyl chains increased cytotoxicity, and it was postulated that the addition of a phenyl ring would enhance hydrophobicity and cytotoxicity. Based on the data, it was determined that MGP derivative **2** was the least toxic, causing 32.11% of deaths. Compounds **4** and **5** exhibited the highest levels of toxicity of 47.64% and 48.21%, respectively. In addition, MGP derivatives (**3** and **8**) were found to be less toxic to brine shrimp. Observations revealed that triphenylmethyl/4-methoxybenzoyl chain derivatives are less cytotoxic than myristoyl/4-*t*-butylbenzoyl chain derivatives. In addition, the cytotoxic effect of alkyl chain derivatives increases with increasing concentration.

As per the drug discovery studio data, the cocrystallized ligand novobiocin of the 4URO receptor (Table 3) interacted with ASN 54, ASP 81, ASP 89, and ARG 144 by hydrogen bond interactions; ARG 84, GLU 58, and ARG 200 by pi-anion/pi-cation interactions; and PRO 87 and ILE 102 by pi-alkyl interactions. In the case of the 4XE3 receptor, the complex ligand clotrimazole was stabilized by a pi-sulfur interaction with CYS 356 by pi-alkyl interactions with amino acid residues of LEU 94, ALA 244 and VAL 291. In addition to the molecular docking between all the synthesized molecules and 4URO, molecule **6** was observed as the best-fitting molecule with a docking energy of −9.8 kcal/moL, followed by compounds **8** and **5** with docking scores of −8.6 kcal/moL and −8.4 kcal/moL, respectively (Table 3) (Zhang et al., 2011). Compound **6** interacted with ASN 54, ASP 57, ALA 61, ILE 86, GLN 91, ALA 98, ARG 200, GLU

Table 3
Molecular docking results of the synthesized molecules against 4URO.

Entry	Dock Score (Kcal/mol)	Interacting Residues	RMSD	RMSF	Lennard-Jones-Short Range: Protein-Ligand (KJ/Mol)	Coulombic-Short Range: Protein-Ligand (KJ/Mol)	Average Radius of gyration	SASA (nm/S^2/ N)
1	−**5.6**	ASN 54, SER 55, ASP 81 by hydrogen bond interactions. ASP 81 by unfavorable acceptor–acceptor interaction.	0.163	0.0674	−0.0125425	−0.0346673	1.6582	114.7077
2	−**7.2**	ARG 144 by hydrogen bond interaction, GLU 58 by pi-anion interaction, ILE 86, PRO 87, ILE 102 by pi-alkyl interaction.	0.178	0.0817	−37.9322	−10.7936	1.6672	116.9757
3	−7.4	ILE 86, PRO 87, ILE 102 by pi-alkyl interaction, TYR 229 by pi-pi interaction.	0.229	0.884	−0.335858	−0.291914	1.6818	129.0015
4	−8.2	ARG 144, ASN 145 by hydrogen bond interaction, ASP 89, GLU 193 by pi-cation interaction, ARG 84, PRO 87, ILE 86, ILE 102, TYR 227 by pi-pi interaction.	0.152	0.078	−18.0879	−0.0175833	1.6472	128.5847
5	−8.4	TYR 229 by hydrogen bond interaction, GLU 58 by pi-anion interaction, ILE 86, ILE 102, ALA 61 by pi-pi interaction, PHE 204 by pi-pi stacked interaction, ASP 57 by pi-sigma interaction.	0.111	0.0818	−0.00109673	0.00146823	1.6449	125.8481
6	−9.8	ARG 84 by hydrogen bond interaction, GLU 58 by pi-anion interaction, PHE 204 by pi-pi stacking interaction, ALA 61, ILE 86, ALA 98, ARG 200 by pi-alkyl interaction.	0.128	0.0733	−10.08751	0.431476	1.6478	124.6634
7	−6.2	GLU 58, ARG 84 by pi-anion interaction, PRO 87 by pi-alkyl interaction.	0.124	0.0655	−0.00115603	0.000529796	1.6471	115.9002
8	−8.6	ARG 84 by hydrogen bond interaction, PRO 87, ILE 86, ILE 51, VAL 79, PHE 204 by pi-alkyl interaction.	0.165	0.0799	−0.0349385	0.00970908	1.6353	124.1911

201, and PHE 204 by different hydrophobic interactions (Fig. 4). The validation of the receptor proteins was also assessed using the Lig-plot and Ramachandran plot through the PDBsum online server (Fig. S9). In the molecular docking analysis of all synthesized molecules and 4XE3 (Table S4), compound **6** was observed to be the best-fitted molecule with a docking energy of −10.9 kcal/moL, followed by compounds **2** and **7** with docking scores of −8.7 kcal/moL and −7.8 kcal/moL, respectively. Compound **6** interacted well with CYS 396 by a pi-sulfur interaction; PHE 296 by a hydrogen bond interaction; SER 295 by an amide-pi stacked interaction; ALA 244 by a pi-sigma interaction; and VAL 93, LEU 94, LEU 396 by pi-alkyl interactions (Fig. 5). In summary, molecular docking study data for the assessment of antibacterial and antifungal activities, 4URO and 4XE3 receptors were used. In the case of the 4URO receptor, compound **6** showed the maximum docking score, and the surrounding residues of compound **6**, such as ARG 84, GLU 58, and ARG 200, were similar to the surrounding residues of novobiocin. In the case of the 4XE3 receptor, compound **6** showed the maximum docking score, and the surrounding residues of compound **6**, such as CYS 356, were similar to the surrounding residues of clotrimazole.

The RMSD values (Almehmadi et al., 2023) of both receptor (4URO/4XE3)-ligand complexes were within 0.11–0.23 nm and 0.144–0.159 nm, respectively (Figs. 6 and 7). In the case of the RMSF data of the 4URO-ligand complex, a significant fluctuation was observed at approximately 1500 atoms with a maximum value of approximately 0.5 nm. In the case of the RMSF data of the 4XE3-ligand complex, significant fluctuations were observed at approximately 1000 atoms and 3000 atoms with a maximum value of approximately 0.3 nm. These RMSF data confirmed that all ligand molecules interacted well with the receptor without disturbing the protein structure integrity. Measurement of R_g values associated with the receptor (4URO/4XE3)-ligand complex was used to determine the integrity of the complex with time. In the case of stable protein structures, the R_g value always maintained a steady result for the full-time scale, and in the case of unfolded proteins, the R_g values fluctuated over time. Higher R_g values correlated with less stability, and lower R_g values indicated more stability of the protein structure. The R_g values of all ligand-receptor (4URO) complexes were within 1.644823–1.659541 nm, and the R_g values of all ligand-receptor (4XE3) complexes were within 1.6451–1.6599 nm.

These data demonstrated the stability of the protein–ligand complex. SASA measurements showed the target protein's solvent-accessible area during dynamics. In this work, the SASA values of the 4URO-ligand complexes were within 114.7077–129.0015 nm/S^2/N, and the SASA values of the 4XE3-ligand complexes were within 114.7077–129.0015 nm/S^2/N. These data confirmed that ligand molecules did not negatively affect the folding of the protein structure. As per the Lennard-Jones potential data table, all receptor-ligand complexes had positive effects on the receptor affinity of the ligand molecules, whereby in the case of coulombic interaction energy data for 4URO receptor 4URO-5 (0.000146823), 4URO-6 (0.431476), 4URO-7 (0.000529796), 4URO-8 (0.00970908) and for 4XE3 receptor 4XE3-1 (0.00126413), 4XE3-3 (0.003529), 4XE3-5 (0.000225823), 4XE3-6 (0.524276), 4XE3-7 (0.0005576), 4XE3-8 (0.0077008) showed less effects on receptor affinity (Ahmad et al., 2017; Kawsar et al., 2022).
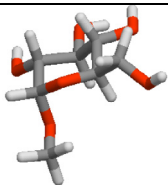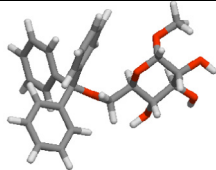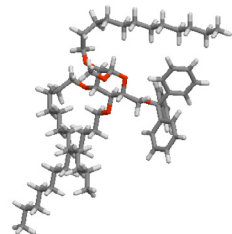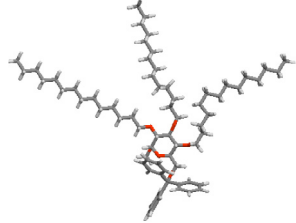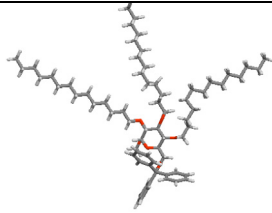
Observation of physicochemical and ADMET profiling data showed that compound **1** demonstrated the maximum probability (0.998) with a water solubility value of 0.087. Compound **4** showed maximum Log P, Log D, blood–brain barrier permeability and human intestinal absorption of 19.625, 4.572, 0.955 and 0.955, respectively. The maximum permeation of Caco-2 cells and plasma protein binding demonstrated that compounds **8** and **6** had values of −4.786 and 82.712, respectively. The maximum drug-induced and mutagenicity displayed by molecule **5** was 0.672 and 0.414, respectively. Compound **7** showed the maximum hepatotoxicity (with a probability value of 0.736) (Table S5). Based on physicochemical and ADMET data, almost all compounds adhered to the Lipinski rule of five. Compounds **1**, **4**, **6** and **8** satisfied all criteria for physicochemical and ADMET data (Afza et al., 2023; Ouassaf et al., 2022).
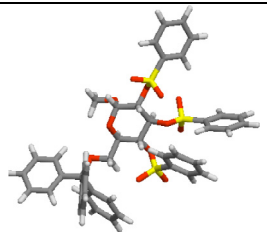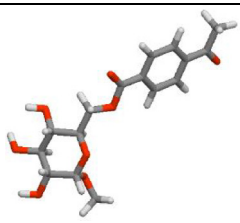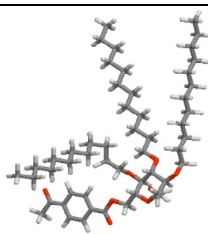
The aforementioned POM theory, in its nascent stage, has been efficaciously expanded to encompass a diverse range of biotargets (Hadda et al., 2021). In this study, we aimed to identify the pharmacophore sites of a series of MGP derivatives **1** to **8**. Based on the physical and chemical characteristics of these analogs, the pharmacophore locations were identified. The Petra, Osiris, and Molinspiration (POM) platform was employed to do this.

The Osiris analysis conducted on compounds **1**–**8** revealed that the majority of the compounds exhibited no adverse effects, with the exception of compound **4**, as indicated in Table S6. Molinspira-

Table 4

Molinspiration calculations of compounds **1**–**8**.

Entry	Geometry and Structure optimization	Calculation of molecular properties	Calculation of bioactivity scores
1		miLogP -2.03 TPSA 99.38 MW 194.18 nOHNH 4 nviolations 0 volume 169.34	GPCR ligand -0.30 Ion channel modulator 0.00 Kinase inhibitor -0.64 Nuclear receptor ligand -0.95 Protease inhibitor -0.44 Enzyme inhibitor 0.36
2		miLogP 3.43 TPSA 88.39 MW 436.50 nOHNH 3 nviolations 0 volume 401.03	GPCR ligand 0.04 Ion channel modulator -0.13 Kinase inhibitor -0.11 Nuclear receptor ligand 0.05 Protease inhibitor 0.11 Enzyme inhibitor 0.42
3		miLogP 10.66 TPSA 55.40 MW 941.48 nOHNH 0 nviolations 2 volume 1008.07	GPCR ligand -3.54 Ion channel modulator -3.73 Kinase inhibitor -3.70 Nuclear receptor ligand -3.68 Protease inhibitor -3.21 Enzyme inhibitor -3.55
4		miLogP 10.85 TPSA 55.40 MW 1025.64 nOHNH 0 nviolations 2 volume 1108.88	GPCR ligand -3.71 Ion channel modulator -3.82 Kinase inhibitor -3.81 Nuclear receptor ligand -3.79 Protease inhibitor -3.62 Enzyme inhibitor -3.71
5		miLogP 10.13 TPSA 106.62 MW 917.15 nOHNH 0 nviolations 2 volume 873.67	GPCR ligand -3.56 Ion channel modulator -3.73 Kinase inhibitor -3.70 Nuclear receptor ligand -3.69 Protease inhibitor -3.27 Enzyme inhibitor -3.57

6		miLogP 7.57 TPSA 157.83 MW 856.99 nOHNH 0 nviolations 3 volume 712.45	GPCR ligand -2.16 Ion channel modulator -3.37 Kinase inhibitor -3.03 Nuclear receptor ligand -3.04 Protease inhibitor -1.48 Enzyme inhibitor -2.43
7		miLogP 0.30 TPSA 122.53 MW 340.33 nOHNH 3 nviolations 0 volume 296.24	GPCR ligand -0.04 Ion channel modulator -0.09 Kinase inhibitor -0.30 Nuclear receptor ligand -0.26 Protease inhibitor -0.06 Enzyme inhibitor 0.17
8		miLogP 10.41 TPSA 89.55 MW 845.30 nOHNH 0 nviolations 2 volume 903.28	GPCR ligand -2.40 Ion channel modulator -3.41 Kinase inhibitor -3.23 Nuclear receptor ligand -3.27 Protease inhibitor -1.80 Enzyme inhibitor -2.80

tion analysis conducted on the MGP compounds indicated the presence of superfluous substituents, as the molecular weight exceeded 500 g/mol. This represents the initial transgression of Lipinski's rule of five. A subsequent infraction will manifest if the calculated logarithm of the partition coefficient (cLogP) exceeds 5. Therefore, compounds **3**, **4**, **5**, **6** and **8** may present a problem of bioavailability (Table 4).

Dithymoquinone has been identified as a promising anti-COVID-19 agent, with an MIC in the nanomolar range, as evidenced by recent research findings (Hadda et al., 2013a, 2013b, 2019). It is noteworthy that a comparison can be made between the pharmacophore site of dithymoquinone (with a distance of dO1–O2 = 4.5 A) and the pharmacophore site of compound **6**, which exhibits antibacterial, antifungal, and antiviral properties (with a distance of dO1–O4 = 4.6 A). The significant resemblance prompted us to proceed expeditiously with the screening of compound **6** for anti-COVID properties. Who can say? It is possible that a pleasant surprise awaits our group (Figs. 9 and S11).

Moreover, it is evident that the presence of aromatic substituents, owing to their high electron density, can significantly augment both the binding affinity and antimicrobial efficacy of MGP. In addition, the ADMET analysis conducted to predict the potential toxicity of the MGP derivatives indicated that all of the compounds exhibit a nontoxic and noncarcinogenic profile. Furthermore, the investigated compounds exhibited encouraging pharmacokinetic characteristics. Further investigations on drug-likeness using *in vitro* and *in vivo* experiments, which also consider nontoxic concentrations toward healthy cells, are likely to be conducted in relation to this fascinating research question. The results indicate that incorporating multiple electron-enriched and electron-deficient groups onto the C-6 position followed by the C-2, C-3, and C-4 positions of MGP structures significantly improves the antimicrobial efficacy of the synthesized MGP derivatives. The outer membrane of gram-negative bacteria is composed of phospholipids that exhibit a purely hydrophobic nature

(Ingólfsson and Andersen, 2011; Walsh et al., 2019; Zhou and Wang, 2020). The compounds underwent modification by attaching a lengthy hydrocarbon chain and an aromatic ring at positions C-6, C-2, C-3, and C-4, thereby conferring hydrophobic interaction capability. Theoretically, it could be assumed that MGP derivatives engaged in hydrophobic interactions with the external phospholipid membrane of bacteria. Computational approaches have demonstrated their efficacy as tools and have yielded noteworthy accomplishments in the area of in silico investigations.

5. Conclusion

The novel MGP derivatives designed in this study displayed potent antimicrobial activity, mainly against bacteria and fungi. The most affected bacterial pathogens were *E. coli*, *P. aeruginosa* and *B. cereus*. Additionally, both fungi *A. niger* and *A. flavus* were markedly inhibited by the derivatives. In fact, compounds **5** and **6** should be considered potential candidates for designing and developing more productive and enhanced antimicrobial agents against several human and plant pathogenic microorganisms. Molecular docking simulation has revealed the binding energy of ligand–protein interactions, which ensures the efficacy of all novel compounds against bacteria and fungi. Compared to parent molecules, the docked complexes of compound **6** against 4URO and 4XE3 demonstrated higher binding scores, with significant non-bonding interactions, in comparison to the parent molecules (**1**). This result firmly supports molecular dynamics investigations up to 2500 ps in a protein pocket and examines the binding stability of the docked complex in trajectory analysis, indicating that the protein–ligand complex is highly stable in biological systems. Additionally, in silico property analysis indicated that compounds **1**, **4**, **6** and **8** fulfilled all the required criteria of physicochemical and ADMET data. Based on the preceding discussion, it can be inferred that compound **6** has the potential to make a valuable contribution to the field of anticancer drug development within the

pharmaceutical industry. However, further research is necessary to substantiate this claim. Finally, a POM study revealed that the anti-fungal and antiviral efficiency of compound **6** bearing the ($O^{\delta-}-O'^{\delta-}$) pharmacophore site(s) can be improved by subtle modification of the terminal substituents.

CRediT authorship contribution statement

Mohammed M. Alanazi: Resources. **Dilipkumar Pal:** Visualization. **Sarkar M.A. Kawsar:** Conceptualization.

Declaration of Competing Interest

The authors declare that they have no known competing financial interests or personal relationships that could have appeared to influence the work reported in this paper.

Acknowledgments

Appendix A. Supplementary data

Supplementary data to this article can be found online at https://doi.org/10.1016/j.jsps.2023.101804.

References

Afza, N., Trivedi, P., Bishnoi, A., Parveen, S., Kumar, S., Banerjee, M., 2023. A convergent multicomponent synthesis, spectral analysis, molecular modeling and docking studies of novel 2H-pyrido[1,2-a]pyrimidine-2,4(3H)-dione derivatives as potential anti-cervical cancer agents. J. Mol. Struct., 134982

Ahmad, S., Raza, S., Uddin, R., Azam, S.S., 2017. Binding mode analysis, dynamic simulation and binding free energy calculations of the MurF ligase from acinetobacter Baumannii. J. Mol. Graph. Model. 77, 72–85.

Ahmad, S.S., Sinha, M., Ahmad, K., Khalid, M., Choi, I., 2020. Study of Caspase 8 inhibition for the management of Alzheimer's disease: a molecular docking and dynamics simulation. Molecules 25 (9), 2071.

Almehmadi, M., Alsaiari, A.A., Allahyani, M., Alsharif, A., Aljuaid, A., Saha, S., Asif, M., 2023. Computational studies and antimicrobial activity of 1-(benzo[d]oxazol-2-yl)-3,5-diphenylformazan derivatives. Curr. Comput. Aided Drug Des. 37403393

Banerjee, P., Eckert, A.O., Schrey, A.K., Preissner, R., 2018. ProTox-II: a webserver for the prediction of toxicity of chemicals. Nucl. Acid Res. 46 (W1), W257–W263.

Bauer, A.W., Kirby, W.M.M., Sherris, J.C., Turck, M., 1966. Antibiotic susceptibility testing by a standardized single disk method. Am. J. Clin. Pathol. 45, 493–496.

Bechlem, K., Aissaoui, M., Belhani, B., Rachedi, K.O., Bouacida, S., Bahadi, R., Djouad, S.E., Mansour, R.B., Bouaziz, M., Almalki, F.A., Hadda, T.B., Berredjem, M., 2010. Synthesis, X-ray crystallographic study and molecular docking of new a-sulfamidophosphonates: POM analyses of their cytotoxic activity. J. Mol. Struct. 1210, 127990.

Berredjem, M., Bouzina, A., Bahadi, R., Bouacida, S., Rastija, V., Djouad, S.E., Sothea, T.O., Almalki, F.A., Hadda, T.B., Aissaoui, M., 2020. Antitumor activity, X- Ray crystallography, in silico study of some-sulfamido-phosphonates. Identification of pharmacophore sites. J. Mol. Struct. 1250, 131886.

Bertozzi, C.R., Kiessling, L.L., 2001. Chemical glycobiology. Science 291, 2357–2364.

Bhat, A.R., Dongre, R.S., Almalki, F.A., Berredjem, M., Aissaoui, M., Touzani, R., Hadda, T.B., Akhter, M.S., 2021. Synthesis, biological activity and POM/DFT/docking analyses of annulated Pyrano[2,3-d]pyrimidine derivatives: Identification of antibacterial and antitumor pharmacophore sites. Bioorg. Chem. 106, 104480.

Bulbul, M.Z.H., Chowdhury, T.S., Misbah, M.M.H., Ferdous, J., Dey, S., Kawsar, S.M.A., 2021. Synthesis of new series of pyrimidine nucleoside derivatives bearing the acyl moieties as potential antimicrobial agents. Pharmacia 68, 23–34.

Chen, S., Fukuda, M., 2006. Cell type-specific roles of carbohydrates in tumor metastasis. Meth. Enzymol. 416, 371–380.

Clinical Laboratory Standards Institute (CLSI), 2012. Methods for Dilution Antimicrobial Susceptibility Tests for Bacteria that Grow Aerobically. Clinical and Laboratory Standards Institute, Wayne, PA, USA.

Daina, A., Michielin, O., Zoete, V., 2017. SwissADME: a free web tool to evaluate pharmacokinetics, drug-likeness and medicinal chemistry friendliness of small molecules. Sci. Rep. 7 (1), 42717.

Farhana, Y., Amin, M.R., Hosen, A., Kawsar, S.M.A., 2021a. Bromobenzoylation of methyl α-D-mannopyranoside: Synthesis and spectral characterization. J. Sib. Fed. Univ. Chem. 14, 171–183.

Farhana, Y., Amin, M.R., Hosen, M.A., Bulbul, M.Z.H., Dey, S., Kawsar, S.M.A., 2021b. Monosaccharide derivatives: Synthesis, antimicrobial, PASS, antiviral, and molecular docking studies against SARS-CoV-2 M^{pro} inhibitors. J. Cellul. Chem. Technol. 55, 477–499.

Grib, I., Berredjem, M., Rachedi, K.O., Djouad, S.E., Bouacida, S., Bahadi, R., Ouk, T.S., Kadri, M., Hadda, T.B., Belhania, B., 2020. Novel N-sulfonylphthalimides: Efficient synthesis, X-ray characterization, spectral investigations, POM analyses, DFT computations and antibacterial activity. J. Mol. Struct. 1217, 12842.

Grover, R.K., Moore, J.D., 1962. In-vitro efficacy of certain essential oils and plant extracts against three major pathogens of *Jatropha curcas* L. Phytopathology 52, 876–879.

Hadda, T.B., Kerbal, A., Bennani, B., Houari, G.A., Daoudi, M., Leite, A.C.L., Masand, V.H., Jawarkar, R.D., Charrouf, Z., 2013a. Molecular drug design, synthesis and pharmacophore site identification of spiroheterocyclic compounds: Trypanosoma crusi inhibiting studies. Med. Chem. Res. 22, 57–69.

Hadda, T.B., Ali, M.A., Masand, V., Gharby, S., Fergoug, T., Warad, I., 2013b. Tautomeric origin of dual effects of N1-nicotinoyl-3-(4'-hydroxy-3'-methyl phenyl)-5-[(sub)phenyl]-2-pyrazolines on bacterial and viral strains: POM analyses as new efficient bioinformatics' platform to predict and optimize bioactivity of drugs. Med. Chem. Res. 22, 1438–1449.

Hadda, T.B., Rauf, A., Zgou, H., Senol, F.S., Orhan, I.E., Mabkhot, Y.N., Althagafi, I.I., Farghaly, T.A., Alterary, S., 2019. Drug design of inhibitors of Alzheimer's disease (AD): POM and DFT analyses of cholinesterase inhibitory activity of β-amino di-carbonyl derivatives. Mini Rev. Med. Chem. 19, 688–705.

Hadda, T.B., Senol, F.S., Orhan, I.E., Zgou, H., Rauf, A., Mabkhot, Y.N., Bennani, B., Emam, D.R., Asayari, N.A.K.A., Muhsinah, A.B., Maalik, A., 2020. Spiro heterocyclic compounds as potential anti-Alzheimer agents (Part 2): their metal chelation capacity, POM analyses and DFT studies. Med. Chem. 16, 1–10.

Hadda, T.B., Deniz, F.S., Orhan, I.E., Zgou, H., Rauf, A., Mabkhot, Y.N., Bennani, B., Emam, D.R., Kheder, N.A., Asayari, A., Muhsinah, A.B., 2021. Spiro heterocyclic compounds as potential anti-alzheimer agents (Part 2): Their metal chelation capacity, POM analyses and DFT studies. Med. Chem. 17, 834.

Hasan, A.H., Murugesan, S., Amran, S.I., Chander, S., Alanazi, M.M., Hadda, T.B., Shakya, S., Pratama, M.R.F., Das, B., Biswas, S., Jamalis, J., 2022. Novel thiophene chalcones-coumarin as acetylcholinesterase inhibitors: Design, synthesis, biological evaluation, molecular docking, ADMET prediction and molecular dynamics simulation. Bioorg. Chem. 119, 105572.

Hosen, M.A., Munia, N.S., Al-Ghorbani, M., Baashen, M., Almalki, F.A., Hadda, T.B., Ali, F., Mahmud, S., Saleh, M.A., Laaroussi, H., Kawsar, S.M.A., 2022. Synthesis, antimicrobial, molecular docking and molecular dynamics studies of lauroyl thymidine analogs against SARS-CoV-2: POM study and identification of the pharmacophore sites. Bioorg. Chem. 125, 105850.

Ingólfsson, H.I., Andersen, O.S., 2011. Alcohol's effects on lipid bilayer properties. Biophys. J. 101, 847–855.

Islam, S., Hosen, M.A., Ahmad, S., ul Qamar, M.T., Dey, S., Hasan, I., Fujii, Y., Ozeki, Y., Kawsar, S.M.A., 2022. Synthesis, antimicrobial, anticancer activities, PASS prediction, molecular docking, molecular dynamics and pharmacokinetic studies of designed methyl α-D-glucopyranoside esters. J. Mol. Struct. 1260, 132761.

Jordheim, L.P., Ben Larbi, S., Fendrich, O., Ducrot, C., Bergeron, E., Dumontet, C., 2012. Gemcitabine is active against clinical multiresistant *Staphylococcus aureus* Strains and is Synergistic with Gentamicin. Int. J. Antimicrob. Agents 39, 444–447.

Joshi, B.C., Juyal, V., Sah, A.N., Saha, S., 2023. Computational investigation of geniposidic acid as an anticancer agent using molecular docking, molecular dynamic simulation, DFT calculation, and OSIRIS-Molinspiration profiling. Phys. Chem. Res. 11, 801.

Judge, V., Narasimhan, B., Ahuja, M., Sriram, D., Yogeeswari, P., Clercq, E.D., Pannecouque, C., Balzarini, J., 2013. Synthesis, antimycobacterial, antiviral, antimicrobial activity and QSAR studies of N(2)-acyl isonicotinic acid hydrazide derivatives. Med. Chem. 9, 53–76.

Kabir, A.K.M.S., Kawsar, S.M.A., Bhuiyan, M.M.R., Islam, M.R., Rahman, M.S., 2004. Biological evaluation of some mannopyranoside derivatives. Bull. Pure Appl. Sci. 23, 83–91.

Kabir, A.K.M.S., Kawsar, S.M.A., Bhuiyan, M.M.R., Rahman, M.S., Banu, B., 2008. Biological evaluation of some octanoyl derivatives of methyl 4,6-O-cyclohexylidene-α-D-glucopyranoside. Chittagong Univ. J Biol. Sci. 3, 53–64.

Kabir, A.K.M.S., Kawsar, S.M.A., Bhuiyan, M.M.R., Rahman, M.S., Chowdhury, M.E., 2009. Antimicrobial screening studies of some derivatives of methyl α-D-glucopyranoside. Pak. J. Sci. Ind. Res. 52, 138–142.

Kawsar, S.M.A., Huq, E., Nahar, N., 2008. Cytotoxicity assessment of the aerial parts of *Macrotyloma uniflorum* Linn. Int. J. Pharmacol. 4, 297–300.

Kawsar, S.M.A., Kumer, A., 2021. Computational investigation of methyl α-D-glucopyranoside derivatives as inhibitor against bacteria, fungi and COVID-19 (SARS-2). J. Chil. Chem. Soc. 66, 5206–5214.

Kawsar, S.M.A., Matsumoto, R., Fujii, Y., Matsuoka, H., Masuda, N., Iwahara, C., Yasumitsu, H., Kanaly, R.A., Sugawara, S., Hosono, M., Nitta, K., Ishizaki, N., Dogasaki, C., Hamako, J., Matsui, T., Ozeki, Y., 2011. Cytotoxicity and glycan-

binding profile of α-D-galactose-binding lectin from the eggs of a Japanese sea hare (Aplysia kurodai). Protein J. 30, 509–519.

Kawsar, S.M.A., Kumer, A., Munia, N.S., Hosen, M.A., Chakma, U., Akash, S., 2022. Chemical descriptors, PASS, molecular docking, molecular dynamics and ADMET predictions of glucopyranoside derivatives as inhibitors to bacteria and fungi growth. Org. Commun. 15, 184–203.

Konze, K.D., Bos, P.H., Dahlgren, M.K., Leswing, K., Tubert-Brohman, I., Bortolato, A., Robbason, B., Abel, R., Bhat, S., 2019. Reaction-based enumeration, active learning, and free energy calculations to rapidly explore synthetically tractable chemical space and optimize potency of cyclin-dependent kinase 2 inhibitors. J. Chem. Inform. Model. 59 (9), 3782–3793.

Kuzmanic, A., Zagrovic, B., 2010. Determination of ensemble-average pairwise root mean-square deviation from experimental B-factors. Biophys. J. 98 (5), 861–871.

Li, W.R., Xie, X.B., Shi, Q.S., 2010. Antibacterial activity and mechanism of silver nanoparticles on Escherichia coli. Appl. Microbiol. Biotechnol. 85, 1115–1122.

Mabkhot, Y.N., Barakat, A., Yousuf, S., Choudhary, M.I., Frey, W., Hadda, T.B., Mubarak, M.S., 2014. Substituted thieno[2,3-b]thiophenes and related congeners: Synthesis, <beta>-Glucuronidase inhibition activity, crystal structure, and POM analyses. Bioorg. Med. Chem. 22, 6715–6725.

Mahmud, S., Biswas, S., Paul, G.K., Mita, M.A., Afrose, S., Hasan, M.R., Shimu, M.S.S., Uddin, M.A.R., Uddin, M.S., Zaman, S., Kibria, K.M.K., Khan, M.A., Emran, T.B., Saleh, M.A., 2021a. Antiviral peptides against the main protease of SARS-CoV-2: A molecular docking and dynamics study. Arab. J. Chem. 14, 103315.

Mahmud, S., Biswas, S., Paul, G.K., Mita, M.A., Promi, M.M., Afrose, M.R., Hasan, S., Zaman, U.M.S., Dhama, K., Emran, T.B., Saleh, M.A., Simal-Gandara, J., 2021b. Plant-based phytochemical screening by targeting main protease of sars-cov-2 to design effective potent inhibitors. Biology 10, 589.

Maowa, J., Hosen, M.A., Alam, A., Rana, K.M., Fujii, Y., Ozeki, Y., Kawsar, S.M.A., 2021a. Pharmacokinetics and molecular docking studies of uridine derivatives as SARS-CoV-2 M^{pro} inhibitors. Phys. Chem. Res. 9, 385–412.

Maowa, J., Alam, A., Rana, K.M., Dey, S., Hosen, A., Fujii, Y., Hasan, I., Ozeki, Y., Kawsar, S.M.A., 2021b. Synthesis, characterization, synergistic antimicrobial properties and molecular docking of sugar modified uridine derivatives. Ovidius Univ. Ann. Chem. 32, 6–21.

McLaughlin, J.L., 1991. Crown-gall tumors in potato discs and brine shrimp lethality: Two simple bioassays for higher plant screening and fractionation. In: Hostettmann, K. (Ed.), Methods in Plant Biochemistry: Assays for Bioactivity. Academic Press, Cambridge MA, USA, pp. 1–32.

Misbah, M.M.H., Ferdous, J., Bulbul, M.Z.H., Chowdhury, T.S., Dey, S., Hasan, I., Kawsar, S.M.A., 2020. Evaluation of MIC, MBC, MFC and anticancer activities of acylated methyl β-D-galactopyranoside esters. Int. J. Biosci. 16, 299–309.

Opoku, F., Govender, P.P., Pooe, O.J., Simelane, M.B., 2019. Evaluating iso-mukaadial acetate and ursolic acid acetate as plasmodium falciparum hypoxanthine-guanine-xanthine phosphoribosyltransferase inhibitors. Biomolecules 9 (12), 861.

Ouassaf, M., Qais, F.A., Belaidi, S., Bakhouch, M., Mohamed, A.S., Chtita, S., 2022. Combined pharmacophore modeling, 3D-QSAR, molecular docking and molecular dynamics study on indolyl-aryl-sulfone derivatives as new HIV1 inhibitors. Acta Chim. Slov. 69, 489–506.

Rachedi, K.T., Ouk, T.S., Bahadi, R., Bouzina, A., Djouad, S.E., Bechlem, K., Zerrouki, R., Hadda, T.B., Almalki, F.A., Berredjem, M., 2019. Synthesis, DFT and POM analyses of cytotoxicity activity of α-amidophosphonates derivatives: Identification of potential antiviral O, O-pharmacophore site. J. Mol. Struct. 1197, 196–203.

Raies, A.B., Bajic, V.B., 2016. In silico toxicology: Computational methods for the prediction of chemical toxicity. Wiley Interdis. Rev.: Comput. Mol. Sci. 6 (2), 147–172.

Rana, K.M., Maowa, J., Alam, A., Hosen, A., Dey, S., Hasan, I., Fujii, Y., Ozeki, Y., Kawsar, S.M.A., 2021. In silico DFT study, molecular docking, and ADMET predictions of cytidine analogs with antimicrobial and anticancer properties. In Silico Pharmacol. 9, 1–24.

Saha, S., Banerjee, S., Ganguly, S., 2010. Molecular docking studies of some novel hydroxamic acid derivatives. Int. J. Chem. Tech. Res. 2, 932–996.

Saha, S., Pal, D., Nimse, S.B., 2021. Indazole derivatives effective against gastrointestinal diseases. Curr. Topics Med. Chem. 22, 1189–1214.

Seeberger, P.H., Werz, D.B., 2007. Synthesis and medical applications of oligosaccharides. Nature 446, 1046–1051.

Shagir, A.C., Bhuiyan, M.M.R., Ozeki, Y., Kawsar, S.M.A., 2016. Simple and rapid synthesis of some nucleoside derivatives: Structural and spectral characterization. Curr. Chem. Lett. 5, 83–92.

Sheikh, J., Hadda, T.B., 2013. Antibacterial, antifungal and antioxidant activity of some new water-soluble b-diketones. Med. Chem. Res. 22, 964–975.

Singh, N., Siddiqi, M.I., 2017. Computational evaluation of glutamine synthetase as drug target against infectious diseases: molecular modeling, substrate-binding analysis, and molecular dynamics simulation studies. Med. Chem. Res. 26, 450–460.

Varki, A., 1993. Biological roles of oligosaccharides: All of the theories are correct. Glycobiology 3, 97–112.

Walsh, D.J., Livinghouse, T., Goeres, D.M., Mettler, M., Stewart, P.S., 2019. Antimicrobial activity of naturally occurring phenols and derivatives against biofilm and planktonic bacteria. Front. Chem. 7, 653.

Waring, M.J., Hadda, T.B., Kotchevar, A.T., Ramdani, A., Touzani, R., Elkadiri, S., Hakkou, A., Bouakka, M., Ellis, T., 2002. 2,3-Bifunctionalized quinoxalines: Synthesis, DNA interactions and evaluation of anticancer, antituberculosis and antifungal activity. Molecules 7, 641–656.

Zhang, J., Shan, Y., Pan, X., Wang, C., Xu, W., He, L., 2011. Molecular docking, 3D-QSAR Studies, and in silico ADME prediction of p-aminosalicylic acid derivatives as neuraminidase inhibitors. Chem. Biol. Drug Design 78 (4), 709–717.

Zhou, C., Wang, Y., 2020. Structure–activity relationship of cationic surfactants as antimicrobial agents. Curr. Opin. Colloid Interface 45, 28–43.